iScience

CellPress
OPEN ACCESS

Article

p53 mitigates the effects of oncogenic HRAS in urothelial cells via the repression of *MCOLN1*

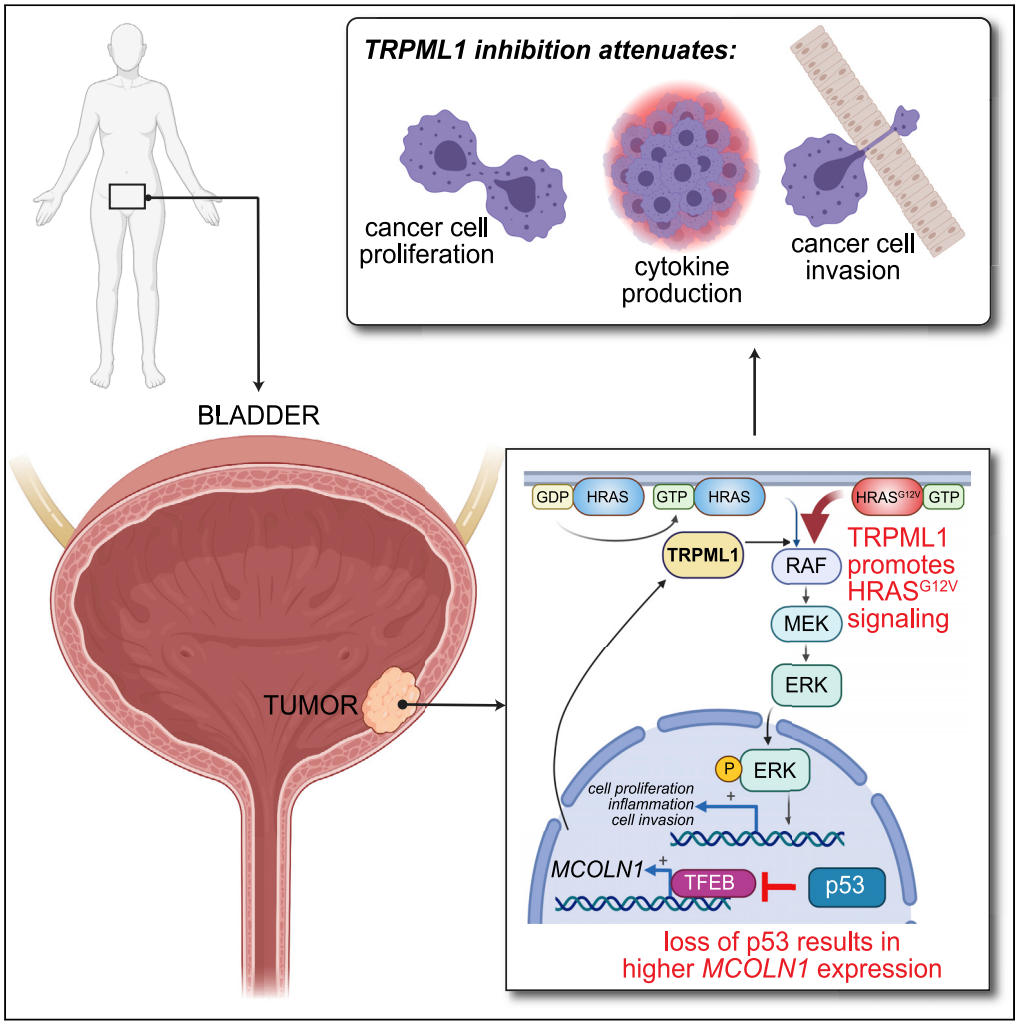

Jewon Jung, Han Liao, Shannon A. Coker, Hong Liang, John F. Hancock, Catherine Denicourt, Kartik Venkatachalam

kartik.venkatachalam@uth.tmc.edu

Highlights

MCOLN1 expression is elevated in BLCA tumors lacking p53

p53 represses *MCOLN1* in both normal and transformed urothelium

MCOLN1 induction upon p53 loss augmented effects of mutant HRAS

Loss of p53 and *HRAS* mutations predict addiction to TRPML1 in bladder cancer

Jung et al., iScience *24*, 102701
July 23, 2021
https://doi.org/10.1016/j.isci.2021.102701

iScience

CellPress
OPEN ACCESS

Article

p53 mitigates the effects of oncogenic HRAS in urothelial cells via the repression of *MCOLN1*

Jewon Jung,[1,4] Han Liao,[1] Shannon A. Coker,[1] Hong Liang,[1] John F. Hancock,[1,2] Catherine Denicourt,[1,2] and Kartik Venkatachalam[1,2,3,5,*]

SUMMARY

Inhibition of TRPML1, which is encoded by *MCOLN1*, is known to deter cell proliferation in various malignancies. Here, we report that the tumor suppressor, p53, represses *MCOLN1* in the urothelium such that either the constitutive loss or ectopic knockdown of *TP53*—in both healthy and bladder cancer cells—increased *MCOLN1* expression. Conversely, nutlin-mediated activation of p53 led to the repression of *MCOLN1*. Elevated *MCOLN1* expression in p53-deficient cancer cells, though not sufficient for bolstering proliferation, augmented the effects of oncogenic HRAS on proliferation, cytokine production, and invasion. Our data suggest that owing to derepression of *MCOLN1*, urothelial cells lacking p53 are poised for tumorigenesis driven by oncogenic HRAS. Given our prior findings that *HRAS* mutations predict addiction to TRPML1, this study points to the utility of TRPML1 inhibitors for mitigating the growth of a subset of urothelial tumors that lack p53.

INTRODUCTION

By coordinating the synthesis and breakdown of macromolecules with signaling events that regulate metabolism, endolysosomes play vital roles in cellular homeostasis (Xu and Ren, 2015). While insufficient endolysosomal function is associated with inborn errors of metabolism, lysosomal storage, and degenerative diseases, increased biogenesis of these organelles is a recurring theme in cancers (Davidson and Vander Heiden, 2017). Several studies have described roles for the endolysosomal cation channel, TRPML1, in different malignancies (Hu et al., 2019; Jung et al., 2019; Kasitinon et al., 2019; Xu et al., 2019; Yin et al., 2019). A common theme in these studies is that TRPML1 is necessary for malignancy-promoting signaling cascades involving RAS-MAPK and mTORC1. For instance, *HRAS*-driven cancers exhibit increased TRPML1 abundance and activity, which underlies endolysosomal exocytosis necessary for recycling cholesterol-rich membranes and oncogenic HRAS to the plasma membrane (Jung and Venkatachalam, 2019; Jung et al., 2019). As a result, TRPML1 inhibition or *MCOLN1* knockdown disrupts ERK activation and cell proliferation in HRAS-driven cancer cells. TRPML1-dependent vesicle exocytosis is also necessary for the release of lysosomal ATP, which in the case of triple-negative breast cancers, stimulates cell migration and metastases (Xu et al., 2019). In other cancers, TRPML1 promotes untrammeled proliferation and tumor growth via mTORC1 (Hu et al., 2019; Xu et al., 2019).

These studies make a compelling argument for understanding the pathways that govern *MCOLN1* expression in cancers. Of major significance here are TFEB, TFE3, and MITF—transcription factors that induce the expression of *MCOLN1* and other endolysosomal genes harboring "coordinated lysosomal expression and regulation" (CLEAR) motifs (Martina et al., 2014; Palmieri et al., 2011; Ploper et al., 2015; Sardiello et al., 2009; Settembre et al., 2011, 2012). Signaling events that influence the nucleocytoplasmic distribution of these transcription factors function as *de facto* regulators of endolysosomal biogenesis (Martina et al., 2012; Medina et al., 2015; Palmieri et al., 2017; Roczniak-Ferguson et al., 2012; Settembre et al., 2011). Several cancers are characterized by either the constitutive localization of TFEB/TFE3/MITF in cell nuclei or by amplifications that upregulate their expression (Argani, 2015; Blessing et al., 2017; Calcagnì et al., 2016; Kauffman et al., 2014; Kundu et al., 2018; Li et al., 2019; Perera et al., 2015, 2019; Ploper et al., 2015). The attendant potentiation of endolysosomal biogenesis supports cancer cell survival, proliferation, and metastases. Because inhibition of TRPML1 arrests proliferation or induces cell death in cancers with elevated expression of the CLEAR network genes (Hu et al., 2019;

[1]Department of Integrative Biology and Pharmacology, McGovern Medical School at the University of Texas Health Sciences Center (UTHealth), Houston, TX 77030, USA

[2]Graduate Program in Biochemistry and Cell Biology, MD Anderson Cancer Center and UTHealth Graduate School of Biomedical Sciences, Houston, TX, USA

[3]Graduate Program in Neuroscience, MD Anderson Cancer Center and UTHealth Graduate School of Biomedical Sciences, Houston, TX, USA

[4]Present address: Department of BioSafety, College of Life and Health Science, Kyungsung University, Busan 48434, Republic of Korea

[5]Lead contact

*Correspondence: kartik.venkatachalam@uth.tmc.edu

https://doi.org/10.1016/j.isci.2021.102701

Jung and Venkatachalam, 2019; Jung et al., 2019), tumors with hyperactivated TFEB/TFE3/MITF signaling are addicted to TRPML1.

Despite all this progress, many questions persist. For instance, we still do not fully understand how the CLEAR network and *MCOLN1* expression are pathologically augmented in cancer. In healthy cells, feedback mechanisms keep endolysosomal biogenesis in check. For instance, mTORC1 suppresses endolysosomal biogenesis by driving phosphorylation and cytosolic retention of TFEB and TFE3 (Martina et al., 2012, 2014; Roczniak-Ferguson et al., 2012; Wang et al., 2015), which is why high mTORC1 activity is correlated with repression of the CLEAR network. In cancers, however, these axes are often dysregulated—a notion exemplified by KRAS-driven pancreatic cancer cells, which exhibit hyperactivation of *both* mTORC1- and TFEB-driven gene expression owing to failure of the mutually inhibitory mechanisms linking these entities (Perera et al., 2015). In addition, genomic landscapes of cancer cells encourage qualitative shifts in the regulatory pathways that control endolysosomal biogenesis. Signaling that normally curtails endolysosomal gene expression morphs into drivers of vesicular biogenesis in cancer. For example, while the tumor suppressor, p53, activates TFEB and TFE3 in normal fibroblasts exposed to DNA damage, loss of p53 in cancers is also associated with the paradoxical activation of the TFEB/TFE3 endolysosome axis (Brady et al., 2018; Tasdemir et al., 2008a, 2008b; Zhang et al., 2017). The lack of clear insights into the regulation of TFEB/TFE3-driven endolysosomal biogenesis hinders our ability to exploit TRPML1 addiction as a therapeutic strategy. To fill the gaps in knowledge, we surveyed *MCOLN1* expression in different cancers using the Cancer Genome Atlas (TCGA) (Cancer Genome Atlas Research Network, 2014). This analysis prompted a focus on bladder carcinoma (BLCA) (Robertson et al., 2017), in which primary tumors exhibited significant elevations in *MCOLN1* expression. Further investigation revealed a role for p53 in repressing TFEB-driven *MCOLN1* expression. Therefore, loss of p53 augmented TRPML1 abundance, which in turn fostered cell proliferation, inflammation, and invasion stemming from oncogenic HRAS. Our study uncovers an axis by which *MCOLN1* expression is regulated and suggests that TRPML1 inhibitors could mitigate tumorigenesis in p53-deficient bladder cancers.

RESULTS

Expression of *MCOLN1* is inversely correlated with p53 targets in bladder cancer

By comparing mRNA levels in tumors relative to matched normal tissues, we found that *MCOLN1* expression was elevated in the TCGA BLCA data set ($\log_2$FC = 0.5, *FDR* = 0.001; Figure 1A and Table S1), which prompted us to select this disease as a suitable model for the identification of cancer-related pathways that depend on *MCOLN1* induction. We also reasoned that ontologies of genes whose transcription correlates with *MCOLN1* would reveal the pathways that depend on *MCOLN1* expression. In BLCA, *MCOLN1* exhibited significant positive and negative correlation with 4737 and 3611 genes, respectively (Figure 1B and Table S2). Targeted gene set enrichment analysis (GSEA) (Subramanian et al., 2005) using the correlation coefficients revealed the expected enrichment of CLEAR targets in genes that are positively correlated with *MCOLN1* (Figure 1C) (Palmieri et al., 2011). Likewise, upon probing the correlation coefficients against MSigDB, we found that genes that positively correlated with *MCOLN1* exhibited enrichment for modules related to lysosomes and lytic vacuoles, endocytosis and phagocytosis, and vesicular exocytosis and secretion (Figures 1D and S1). In addition, *MCOLN1* expression was positively correlated with genes that are upregulated during ultraviolet (UV)-induced DNA repair and negatively correlated with p53 target genes and genes that are repressed during UV-induced DNA repair (Figures 1D and S1).

MCOLN1 expression was elevated in primary BLCA tumors with *TP53* mutations

Next, we applied the principles of information theory (Shannon, 1948) to determine whether mutations in any of the 722 genes belonging to the Cancer Gene Census (https://cancer.sanger.ac.uk/census; Table S3) correlated with *MCOLN1* expression in BLCA. We sought to identify those genes that were mutated in tumors with either high or low *MCOLN1* expression, such that partitioning the set of tumors on the basis of *MCOLN1* expression would decrease the stochasticity associated with the appearance of mutations (i.e., an increase in "Shannon information," see STAR methods). We found that 145 genes exhibited significant information gain upon partitioning the tumors on the basis of *MCOLN1* expression (Figure 2A and Table S4). Of these genes, only four (*TP53*, *KDM6A*, *ARID1A*, *RB1*) were mutated in $\geq$15 tumors (Figure 2A). To validate further the relationship between *MCOLN1* expression and mutations in these four genes, we performed targeted GSEA by ranking BLCA tumors on the basis of *MCOLN1* expression. This analysis revealed that mutations in *TP53* ($TP53^{mut}$) and *RB1* ($RB1^{mut}$) were significantly enriched in tumors with highest *MCOLN1* expression, whereas wild-type alleles of both genes ($TP53^{wt}$ and $RB1^{wt}$) were

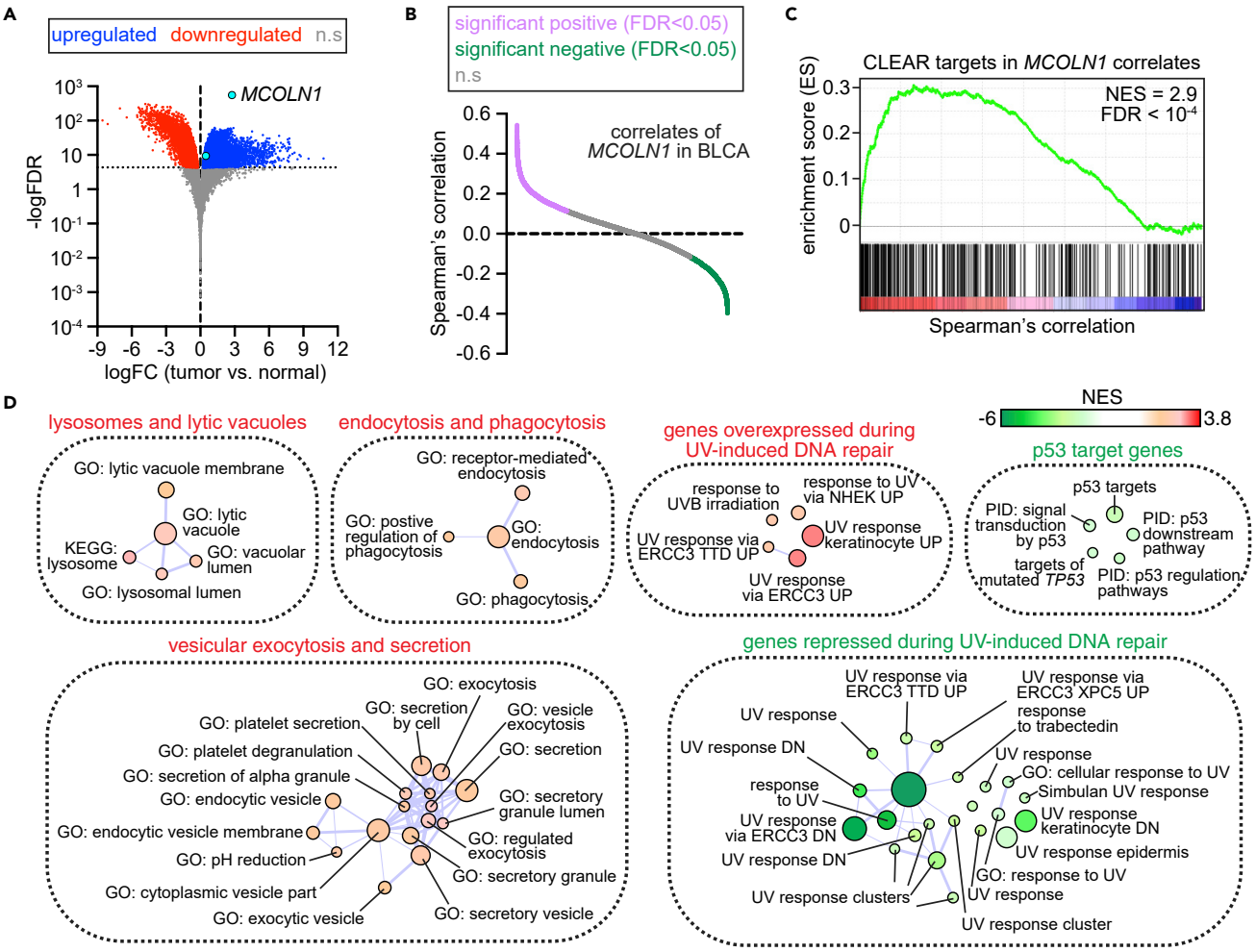

Figure 1. Pathways correlated with *MCOLN1* expression in BLCA

(A) Volcano plot showing DEGs in BLCA primary tumors relative to matched normal tissues. Genes that were significantly (FDR<0.05) upregulated and downregulated in tumors are depicted by blue and red dots, respectively. *MCOLN1* (light blue circle) belonged to the set of significantly upregulated genes. Gray dots represent genes whose expression was not significantly altered in tumors.

(B) Plot showing correlation of 20,177 genes with *MCOLN1*. Values on the Y axis represent Spearman's correlation. Genes that showed significant (FDR <0.05) positive and negative correlation with *MCOLN1* are represented by magenta and green dots, respectively. Gray dots represent genes that were not significantly correlated with *MCOLN1*.

(C) GSEA shows enrichment for CLEAR targets in genes that showed significant positive correlation with *MCOLN1*.

(D) Functional annotation of genes that were significantly correlated with *MCOLN1* in BLCA. All the genes that were significantly correlated with *MCOLN1* were subjected to GSEA. Sets with GSEA FDR<0.05 are shown as nodes. Node color represents NES from GSEA. Node size represents number of genes that make up that set. Thickness of the lines connecting the nodes indicates extent of overlap. Unconnected nodes have no overlap. Abbreviations: FC, fold change; NES, normalized enrichment score.

enriched in tumors with lowest *MCOLN1* expression (Figure 2B). In agreement, pairwise comparison of normalized *MCOLN1* FPKM revealed significantly higher values in $TP53^{mut}$ and $RB1^{mut}$ in comparison with $TP53^{wt}$ and $RB1^{wt}$ tumors, respectively (Figure 2C). In contrast, neither were the mutations in *ARID1A* ($ARID1A^{mut}$) or *KDM6A* ($KDM6A^{mut}$) enriched in tumors with either the highest or lowest *MCOLN1* expression nor was *MCOLN1* expression significantly altered in $ARID1A^{mut}$ or $KDM6A^{mut}$ tumors relative to tumors with wild-type alleles of these two genes ($ARID1A^{WT}$ or $KDM6A^{WT}$, respectively) (Figures 2B and 2C). Together, these data point to elevated *MCOLN1* expression in tumors harboring *TP53* and *RB1* mutations. Because tumors with *RB1* mutations belonged to the larger set with *TP53* mutations (Figure S2), we conclude that tumors harboring *TP53* mutations constitute the broadest set of samples with elevated *MCOLN1* expression.

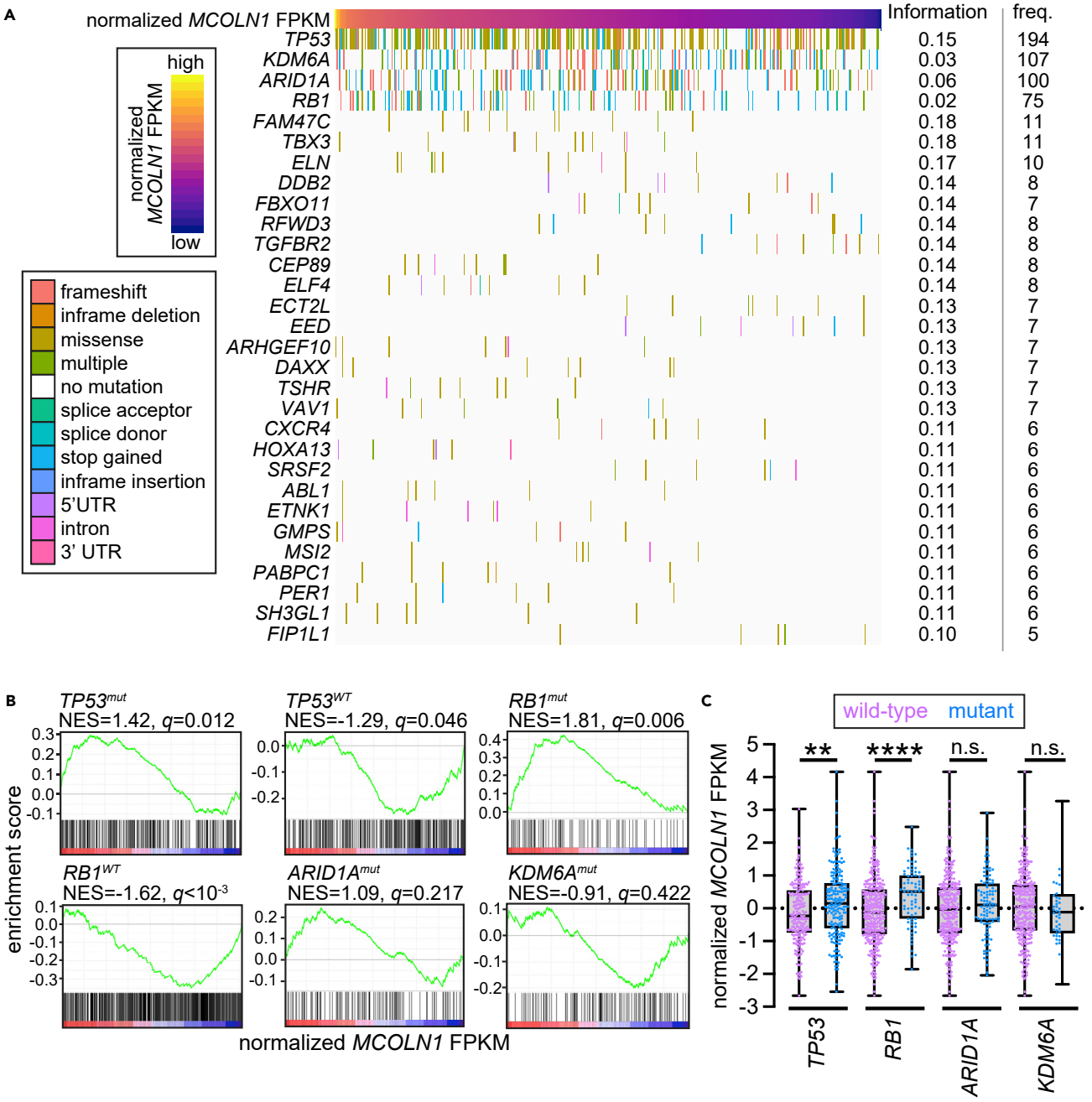

Figure 2. *MCOLN1* expression is elevated in *TP53*^{mut} BLCA tumors

(A) Waterfall plot showing mutations in 30 genes with significant information gain. *MCOLN1* expression is depicted as median normalized FPKM values at the top. Bars mark tumors harboring mutations in respective genes, and bar colors represent the type of mutation. On the right, Shannon information associated with partitioning tumors into three groups based on *MCOLN1* expression are show; and "freq." depicts number of tumors in the BLCA data set that exhibit mutations in the respective genes. For all the genes shown, $Q < 0.0001$.

(B) GSEA traces show enrichment for indicated mutations in tumors ranked on the basis of *MCOLN1* expression (represented as median normalized FPKM values).

(C) Box plots showing *MCOLN1* expression (represented as median normalized FPKM values) in BLCA sorted on the basis of the presence or absence of mutations in the indicated genes. Each dot represents the values from a different tumor and lines in the box plots represent median values. **, $p < 0.01$, t test; ****, $p < 0.0001$, Mann-Whitney tests. Abbreviation: NES, normalized enrichment score; *q*, FDR value; n.s., not significant.

Approximately 47% of BLCA tumors in the TCGA data set were $TP53^{mut}$. Using the IARC database (https://p53.iarc.fr/Default.aspx) (Bouaoun et al., 2016), we found that among the $TP53^{mut}$ BLCA tumors, ~86% harbored *TP53* mutations ($TP53^{trans\text{-}mut}$) that predicted to result in loss of transactivation function owing to either nonsense mutations leading to premature termination or missense mutations in the DNA-binding domain. Among the remainder, ~7% harbored *TP53* mutations ($TP53^{trans\text{-}norm}$) that were either unlikely to affect transactivation or have remained unclassified. Another ~3% carried *TP53* mutations in splice acceptor or donor sites ($TP53^{splice}$), and ~3% harbored multiple *TP53* mutations. Finally, one tumor harbored an inframe mutation. In sum, majority of *TP53* mutations in BLCA were predicted to result in loss of p53 transactivation. Analyses of the RNA sequencing data revealed that in comparison to the values in $TP53^{WT}$ tumors, *MCOLN1* expression was significantly higher in $TP53^{trans\text{-}mut}$ tumors, but not in $TP53^{trans\text{-}norm}$ or $TP53^{splice}$ tumors (Figure S3A). Furthermore, targeted GSEA revealed that $TP53^{trans\text{-}mut}$ mutations were significantly enriched in tumors with high *MCOLN1* expression (Figure S3B). Therefore, *MCOLN1* expression was elevated in tumors that harbored mutations in the DNA-binding domain of p53.

MCOLN1 expression is elevated in p53-deficient bladder cancer cell lines

Next, we sought to examine the relationship between p53 and *MCOLN1* expression in both bladder cancer and healthy urothelial cells. We made use of five different bladder cancer cell lines—HT1197, RT4, SW780, 5637, and T24 (Bubeník et al., 1973; Fogh, 1978; Rasheed et al., 1977; Rigby and Franks, 1970). As per the Cancer Cell Line Encyclopedia (CCLE), HT1197, RT4, and SW780 cells are wild type for *TP53*, whereas 5637 cells harbor a missense *TP53* mutation that is predicted to encode a transactivation-deficient (R280T) variant, and T24 cells are homozygous for a nonsense mutation in the *TP53*-coding sequence that is predicted to yield a null allele (Table S5). In agreement with CCLE, we detected p53 protein in extracts from HT1197, RT4, SW780, and 5637 cells, but not in extracts from T24 cells (Figures S4A and S4B). Interestingly, p53 abundance was higher in 5637 cells relative to RT4 and SW780 (Figure S4A). Application of the p53-stabilizing agent, nutlin (Vassilev et al., 2004), led to a significant increase in p53 protein in RT4 cells but a relatively smaller increase in 5637 cells (Figure S4A). These data suggest that basally higher p53 in 5637 cells involves compensatory upregulation of the protein via the Mdm2–p53 axis targeted by nutlin (Vassilev et al., 2004). Using RT-PCR, we found that in comparison to the values in HT1197, RT4, SW780, or 5637, *MCOLN1* expression was significantly higher in T24 cells (Figure 3A). Therefore, loss of p53 in bladder cancer cells was associated with higher *MCOLN1* expression.

To analyze further the regulation of *MCOLN1* expression by p53 in the bladder cancer cells, we first examined the consequences of knocking down of *TP53* expression. Application of *TP53* siRNA (Xu et al., 2009), which elicited the expected decrease in p53 protein abundance in HT1197, RT4, SW780, or 5637 cells (Figures S4B and S4C), significantly elevated *MCOLN1* expression in those cells (Figure 3A). Conversely, activation of p53 by application of nutlin (Vassilev et al., 2004) decreased *MCOLN1* expression in HT1197, SW780, and RT4 cells (Figure 3B), all of which carry wild-type alleles of *TP53*. Nutlin did not repress *MCOLN1* in the p53-deficient, T24 cells (Figure 3B), which indicates that nutlin lowered *MCOLN1* mRNA via p53. Consistent with TFEB being a transcriptional activator of *MCOLN1* (Sardiello et al., 2009), knockdown of *TFEB* in T24 cells restored *MCOLN1* expression to control levels (Figure S4D). Furthermore, simultaneous knockdown of *TFEB* dampened the extent of *MCOLN1* induction stemming from *TP53* knockdown in RT4 cells (Figure S4E). We also asked whether the role for p53 in *MCOLN1* repression is an exclusive feature of transformed cells or whether p53 restrict *MCOLN1* expression even in healthy, noncancerous urothelial cells. Examination of healthy urothelial cells revealed that knockdown of *TP53*, which led to the expected decrease in p53 abundance (Figures S4B and S4C), augmented *MCOLN1* expression in those cells (Figure 3C). Furthermore, application of nutlin lowered *MCOLN1* expression in the healthy urothelial cells (Figure 3D). Taken together, our data indicate that p53 is necessary and sufficient to regulate *MCOLN1* expression in both healthy urothelial and transformed bladder cancer cells.

The human genome encodes two other *MCOLN1* paralogs called *MCOLN2* and *MCOLN3* (Karacsonyi et al., 2007; Di Palma et al., 2002). Interestingly, both *MCOLN2* and *MCOLN3* exhibited increased expression in T24 cells compared with HT1197, RT4, and SW780 cells (Figure S4F). Arguing against a role for p53 in the regulation of the *MCOLN1* paralogs, however, was our finding that knockdown of *TP53* did not alter *MCOLN2* expression in HT1197, RT4, and SW780 cells (Figure S4F). *MCOLN3* expression, though insensitive to *TP53* knockdown in HT1197 and RT4 cells, was slightly elevated upon application of *TP53* siRNA in SW780 cells (Figure S4F). On the whole, these data indicate that while *MCOLN1* expression in bladder

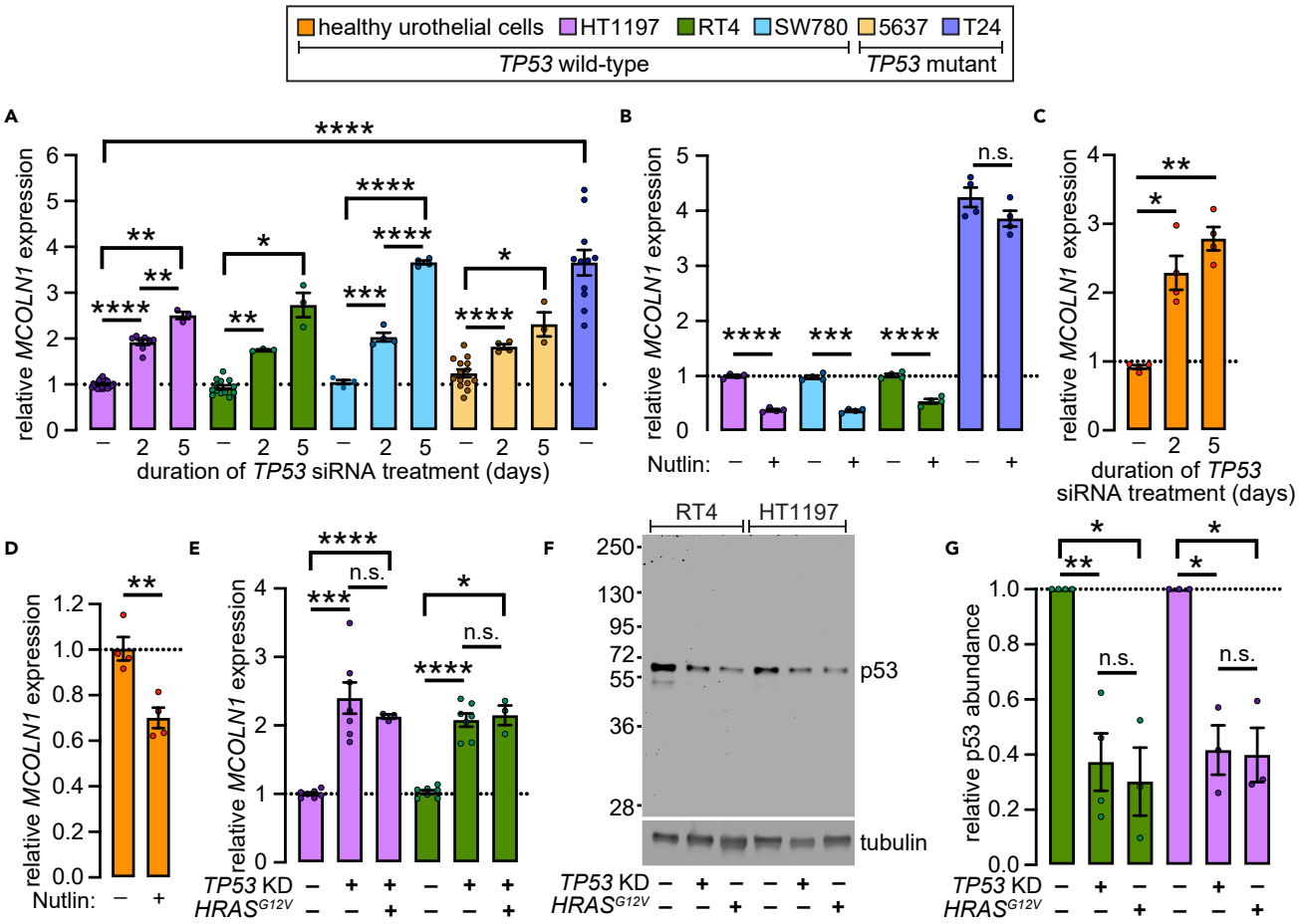

Figure 3. p53 has a necessary and sufficient role in repressing *MCOLN1* in both transformed and healthy urothelial cells

(A) Bar graph showing relative *MCOLN1* expression in the indicated bladder cancer cell lines treated with control siRNA or siRNA against *TP53* (75 nM) for either 2 or 5 days. For each cell type values were normalized to HT1197 control mean. Circles represent independent biological repeats and the values shown represent mean ± SEM; *, $p < 0.05$; **, $p < 0.01$; ****, $p < 0.0001$, t-tests with Bonferroni correction in case of samples used in multiple pairwise comparisons.

(B) Bar graph showing relative *MCOLN1* expression in the indicated bladder cancer cell lines with or without treatment with 10 μM Nutlin for 48 h. For each cell line, values were normalized to cell numbers in the untreated cohorts. Circles represent independent biological repeats and the values shown represent mean ± SEM; ****, $p < 0.0001$,; n.s., not significant, t-tests.

(C) Same as in (A) but in healthy urothelial cells.

(D) Same as in (B) but in healthy urothelial cells.

(E) Same as in (A) but with or without addition of *TP53* siRNA (*TP53* KD) and expression of $HRAS^{G12V}$ as indicated below the graph.

(F) Representative Western blot showing p53 and tubulin abundance in extracts generated from the cell lines indicated above the blot that were treated as indicated below the blot.

(G) Quantification of the data shown in (F). Circles represent independent biological repeats and the values shown represent mean ± SEM; *, $p < 0.05$; **, $p < 0.01$; n.s., not significant, t-tests with Bonferroni correction in case of samples used in multiple pairwise comparisons.

cancer cells was clearly dependent on p53, expression of *MCOLN2* and *MCOLN3* were relatively insensitive to *TP53* knockdown.

Forced expression of oncogenic *HRAS* lowered p53 abundance in bladder cancer cells

We previously demonstrated the existence of an evolutionarily conserved axis by which *MCOLN1* expression was elevated in cells expressing oncogenic *HRAS* (Jung and Venkatachalam, 2019; Jung et al., 2019). In agreement with our previous findings, forced expression of $HRAS^{G12V}$ by lentiviral transduction in HT1197, RT4, SW780, and 5637 cells increased *MCOLN1* expression to extents comparable with those elicited by *TP53* knockdown (Figures 3E and S4G). Knockdown of *TP53* in cells that ectopically expressed $HRAS^{G12V}$ did not increase further the levels of *MCOLN1* mRNA (Figure 3E). The lack of additivity raised the possibility

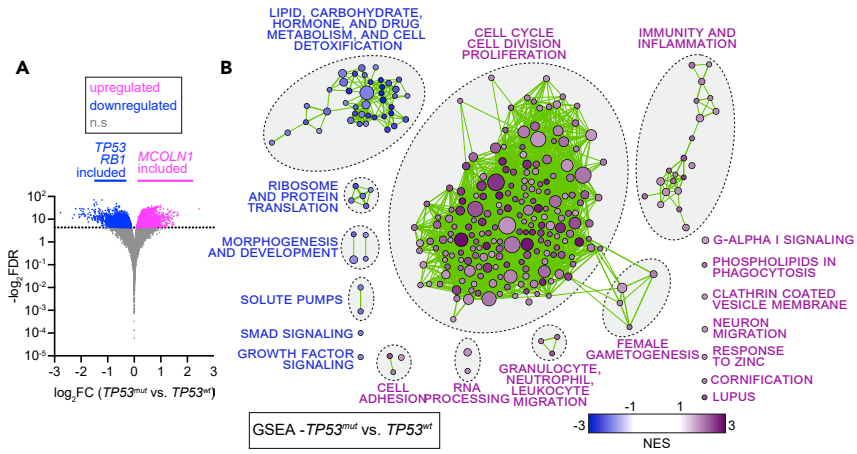

Figure 4. Transcriptional alterations in BLCA tumors harboring *TP53* mutations

(A) Volcano plot showing DEGs in $TP53^{mut}$ compared with $TP53^{wt}$ tumors. Genes that were significantly (FDR <0.05) upregulated and downregulated in $TP53^{mut}$ tumors are depicted by magenta and blue dots, respectively. *MCOLN1* belonged to the set of genes upregulated genes, whereas *TP53* and *RB1* belonged to the set of downregulated genes. Gray dots represent genes whose expression was not significantly altered.

(B) Functional annotation of DEGs in $TP53^{mut}$ relative to $TP53^{wt}$ BLCA tumors. All DEGs were subjected to GSEA. From the results of this analysis, only the gene sets with GSEA FDR <0.05 are shown as nodes. Node color represents NES from GSEA. Node size represents number of genes that make up that set. Thickness of the lines connecting the nodes indicates extent of overlap. Unconnected nodes have no overlap. Abbreviations: FC, fold change.

that $HRAS^{G12V}$ and *TP53* knockdown increased *MCOLN1* expression via the same pathway—a notion consistent with the findings that activating mutations in *HRAS* lead to p53 destabilization (Ries et al., 2000). In agreement, p53 abundance was significantly decreased in bladder cancer cells that ectopically expressed $HRAS^{G12V}$ (Figures 3F and 3G). Because the decrease in p53 induced by $HRAS^{G12V}$ was comparable with that elicited by *TP53* knockdown, our data are consistent with the notion that $HRAS^{G12V}$ promotes *MCOLN1* expression by lowering p53 abundance.

Roles for TRPML1 in proliferation and prevention of cell cycle arrest in p53-deficient bladder cancer cells

Next, we identified the genes whose expression was significantly different in $TP53^{mut}$ tumors relative to those that were $TP53^{wt}$. At FDR<0.05, we identified 5659 differentially expressed genes (DEGs). *MCOLN1* belonged to the cohort of significantly upregulated genes in $TP53^{mut}$ tumors, whereas expressions of both *TP53* and *RB1* were significantly diminished (Figure 4A and Table S6). GSEA identified several functional modules in the DEGs including those related to positive regulation of cell cycle progression and proliferation and immunity and inflammation (Figure 4B and Table S7). Additional upregulated modules comprised gene sets for cell adhesion, RNA processing, and response to zinc (Figure 4B and Table S7). Downregulated modules involved those related to detoxification/drug metabolism via cytochrome p450, hormone signaling, lipase activity, ribosome and protein translation, and solute pumps (Figure 4B and Table S7).

Because modules related to cell cycle progression were upregulated in $TP53^{mut}$ tumors, we asked whether TRPML1 might be necessary for the proliferation of bladder cancer cells lacking p53. In agreement with our previous findings (Jung et al., 2019), the MTT cell proliferation assay revealed that pharmacological inhibition of TRPML1 by application of ML-SI1 (Samie et al., 2013) for 2 days significantly attenuated T24 cell proliferation (Figure 5A). HT1197, RT4, and SW780 cells were much less sensitive to TRPML1 inhibition (Figure 5A). Extending the duration of ML-SI1 treatment to 5 days led to even greater attenuation of T24 cell numbers compared with the effect of the drug on HT1197, RT4, or SW780 cells (Figure 5A). To rule out the possibility that the antiproliferative effects of ML-SI1 reflect a specific influence on the MTT assay, we assessed colony formation. ML-SI1 application led to significantly greater reduction in the number of colonies in T24 relative to HT1197 (Figure 5B). In agreement with our findings using ML-SI1, *MCOLN1* knockdown curtailed the proliferation of T24 cells to a significantly greater extent than it did in HT1197,

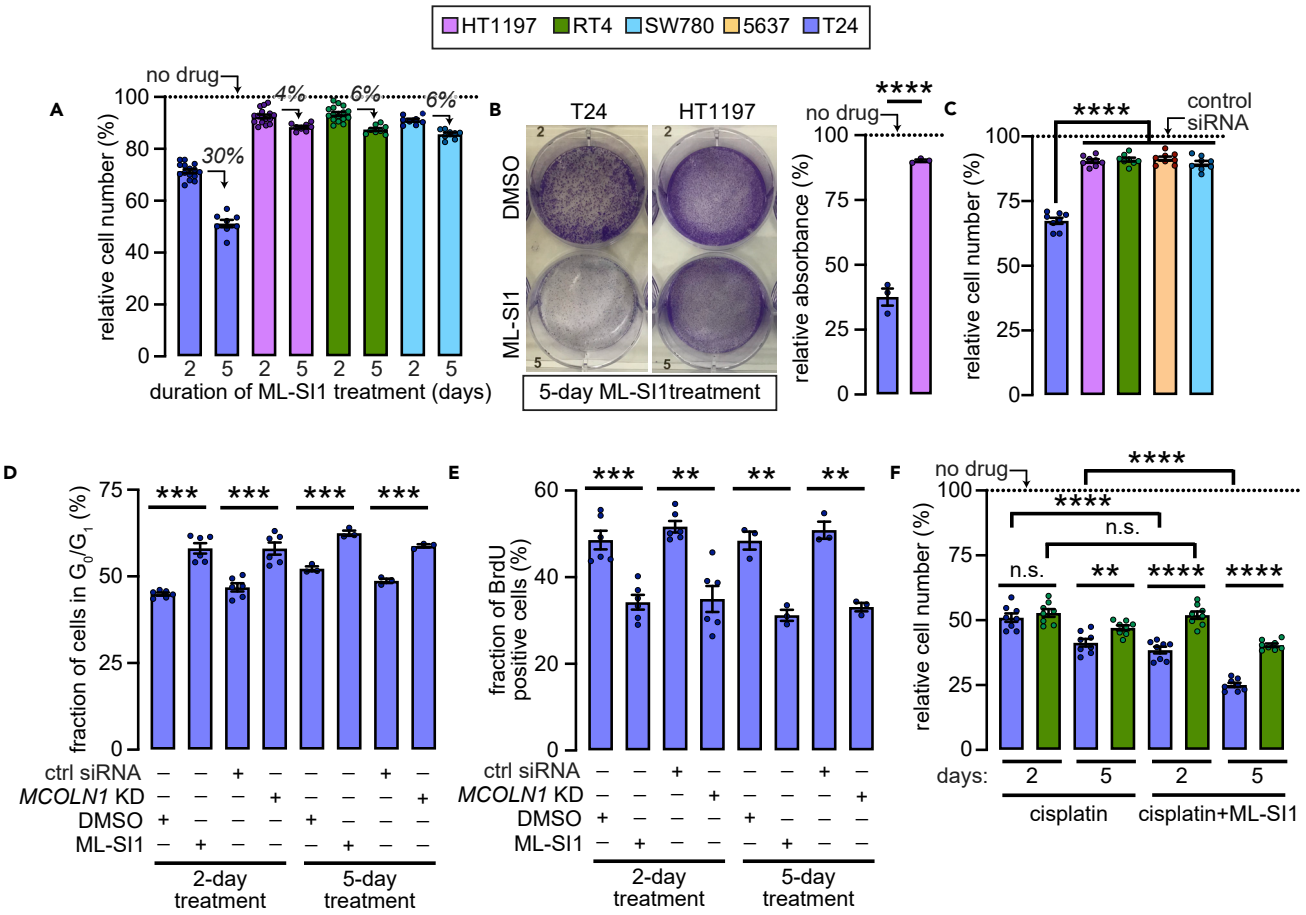

Figure 5. TRPML1 is required for the proliferation of T24, but not HT1197, RT4, SW780 or 5637 bladder cancer cells

(A) Bar graph showing relative number of the indicated cells assessed using the MTT cell proliferation assay. Numbers at the bottom represent duration of 10 μM ML-SI1 application in days. Circles represent independent biological repeats and the values shown represent mean ± SEM.

(B) *Left*, representative images of the indicated cell lines treated with DMSO or 10 μM ML-SI1 for 5-days. Cells grown on the dished were stained with crystal. *Right*, bar graph showing intensity of crystal violet staining in ML-SI1 treated cells normalized to the values in untreated cells. Circles represent independent biological repeats and the values shown represent mean ± SEM; ****, $p < 0.0001$, t test.

(C) Same as (A) but with 200 nM *MCOLN1* siRNA. ****, $p < 0.0001$, t test with Bonferroni tests in case of samples used in multiple pairwise comparisons.

(D) Bar graph showing fraction of T24 cells in the G_0/G_1 phase of the cell cycle in response to the indicated treatments for the indicated durations. Circles represent independent biological repeats and the values shown represent mean ± SEM; ***, $p < 0.001$, t-tests.

(E) Same as (D) but showing BrdU-labeled cells. **, $p < 0.01$; ***, $p < 0.001$, t-tests. Drug concentrations in (D) and (E), 200 nM *MCOLN1* siRNA and 10 μM ML-SI1.

(F) Same as in (A) but in the indicated cell lines for the indicated drugs and for the indicated durations. **, $p < 0.01$; ****, $p < 0.0001$, t-tests. Concentrations, 10 μM cisplatin and 10 μM ML-SI1. Abbreviations: n.s., not significant.

RT4, SW780, or 5637 cells (Figure 5C). Ruling out the possibility that the efficacy of *MCOLN1* siRNA varies between the cell types, extent of *MCOLN1* knockdown in HT1197, RT4, and 5637 cells (~50%, Figure S5A) was in the same range as that elicited by this siRNA in T24 cells (Jung et al., 2019).

Analysis of the fractions of T24 cells in various stages of cell cycle revealed that *MCOLN1* knockdown or TRPML1 inhibition led to a significant increase in the fraction of cells in the G_0/G_1 phase of the cell cycle (Figure 5D). Accumulation of cells in G_0/G_1 was evident within 2 days of treatment and persisted at the 5-day mark (Figure 5D). The larger fraction of cells in G_0/G_1 was accompanied with a decline in the fraction of BrdU-labeled cells (Figure 5E) and cells in the G_2/M phases (Figure S5B). Therefore, the decline in T24 cancer cell numbers upon the knockdown or inhibition of TRPML1 was a consequence of accumulation in the G_0/G_1 phase of the cell cycle with an attendant decline in the fractions in S and G_2/M phases.

Because ML-SI1 slowed progression through the cell cycle, we did not anticipate the drug to synergize with a cytotoxic agent. Indeed, cisplatin decreased the number of T24 and RT4 cells to similar extents (Figure 5F). Treatment with a combination of ML-SI1 and cisplatin led to a further decline in T24, but not RT4 cell numbers (Figure 5F). Normalization to the effects of ML-SI1 showed that sensitivity toward cisplatin treatment was not synergistically enhanced by TRPML1 inhibition (Figure S5C). Neither did cisplatin change the expression of *MCOLN1* (Figure S5D). Thus, ML-SI1 and cisplatin exert their effects on cancer cell number via distinct pathways leading to an additive effect upon simultaneous application of both drugs.

TRPML1-dependent cytokine production regulates cell proliferation, cell invasion, and immune microenvironment in bladder cancers

Given the induction of *MCOLN1* and inflammation in $TP53^{mut}$ BLCA tumors (Figure 4), we asked whether TRPML1 could be participating in cytokine gene expression. We focused our attention on genes encoding IL6 and TNFα, which are involved in various aspects of tumorigenesis (Caetano et al., 2016; Mantovani et al., 2017; Wu and Zhou, 2010). Suggesting a relationship between *MCOLN1* and cytokine gene expression, top half of the tumors in the TCGA BLCA dataset, sorted on the basis of *MCOLN1* expression, also expressed significantly higher levels of *TNF* and *IL6* than did the remainder of the tumors (Figure S6A). In agreement, T24 cells expressed significantly higher levels of *IL6* and *TNF* than did HT1197, RT4, and SW780 cells (Figure 6A). Knockdown of *RELA*, which encodes the p65 subunit of NF-κB (Nolan et al., 1991), partially attenuated *IL6* and *TNF* transcription in all cell types except SW780 (Figure 6A). Notably, application of ML-SI1 or *MCOLN1* knockdown mitigated the expression of the two cytokines in T24 cells to the levels that were typical of HT1197, RT4, and SW780 cells (Figure 6A). These data indicate that cytokine gene expression in p53 deficient bladder cancer cells requires functional NF-κB and TRPML1.

To assess the influence of TNFα on the bladder cancer cell proliferation, we applied a TNFα chelating drug, etanercept (Suffredini et al., 1995), to T24, HT1197, RT4, and SW780 cells. Although all four lines were sensitive to etanercept, T24 cell numbers declined by significantly greater extents than did the others (Figures S6B and 6B). Moreover, simultaneous application of etanercept and ML-SI1 induced a further decline of cell number in T24 but not RT4, HT1197, or SW780 cells (Figure 6B). These data argue in favor of a role for *TNF*, whose expression depended on TRPML1, in promoting the proliferation of bladder cancer cells in an autocrine manner. When grown on Matrigel, significantly larger number of T24 cells (TNFα high) invaded the matrix than did RT4 cells (TNFα low) (Figure 6C). Morphology of cells within the matrix also differed between the two lines. RT4 cells formed tightly packed clusters of 10–20 cells, whereas T24 cells invaded as individuals with typical mesenchymal morphology (Figure 6C). Knockdown of *MCOLN1* in T24 cells decreased the number of invading cells, and the cells that permeated the matrix had acquired morphologies resembling those of RT4 cells, that is elevated cell–cell association (Figure 6C). Given the established roles for TNFα in metastases (Rossi et al., 2018; Wu and Zhou, 2010; Zhu et al., 2014), our data are consistent with TRPML1 regulating the invasiveness of bladder cancer cells via the regulation of *TNF* expression.

IL6 modulates the immune microenvironment of tumors by forcing tumor-associated macrophages (TAMs) to adopt the antiinflammatory and protumorigenic M2 state (Caetano et al., 2016; Chen et al., 2018; Fu et al., 2017; Mantovani et al., 2017). Using CIBERSORT (Newman et al., 2015), we found that tumors in the top half of *MCOLN1* expression harbored a significantly higher density of M2 macrophages and lower density of activated dendritic cells than did tumors with lower *MCOLN1* expression (Figures S6C and 6D). Enrichment for M2 TAMs also correlated with higher *IL6* expression (Figure S6C). Therefore, BLCA tumors with higher *MCOLN1* and *IL6* expression exhibited a protumorigenic immune signature consistent with higher densities of M2 TAMs.

TRPML1 plays a permissive, but not sufficient, role in the regulation of proliferation and inflammation in bladder cancer cells

So far, we have shown roles for TRPML1 in promoting proliferation, invasion, and cytokine expression. Furthermore, knockdown of wild-type *TP53* in HT1197, RT4, SW780, and 5637 cells was sufficient to increase *MCOLN1* expression. These data prompted us to ask whether increased *MCOLN1* expression in *TP53* knockdown cells would be sufficient to augment proliferation and cytokine gene expression. However, treatment of HT1197, RT4, and SW780 cells with *TP53* siRNA increased neither the rates of cell proliferation nor the sensitivity to ML-SI1 (Figure 7A). Similarly, *TP53* knockdown alone did not elevate *IL6* or *TNF* mRNA levels in HT1197, RT4, and SW780 bladder cancer cells (Figure 7B). These data demonstrate that increased *MCOLN1* expression upon loss of p53 plays a strictly permissive role in bladder cancer cell proliferation and inflammation.

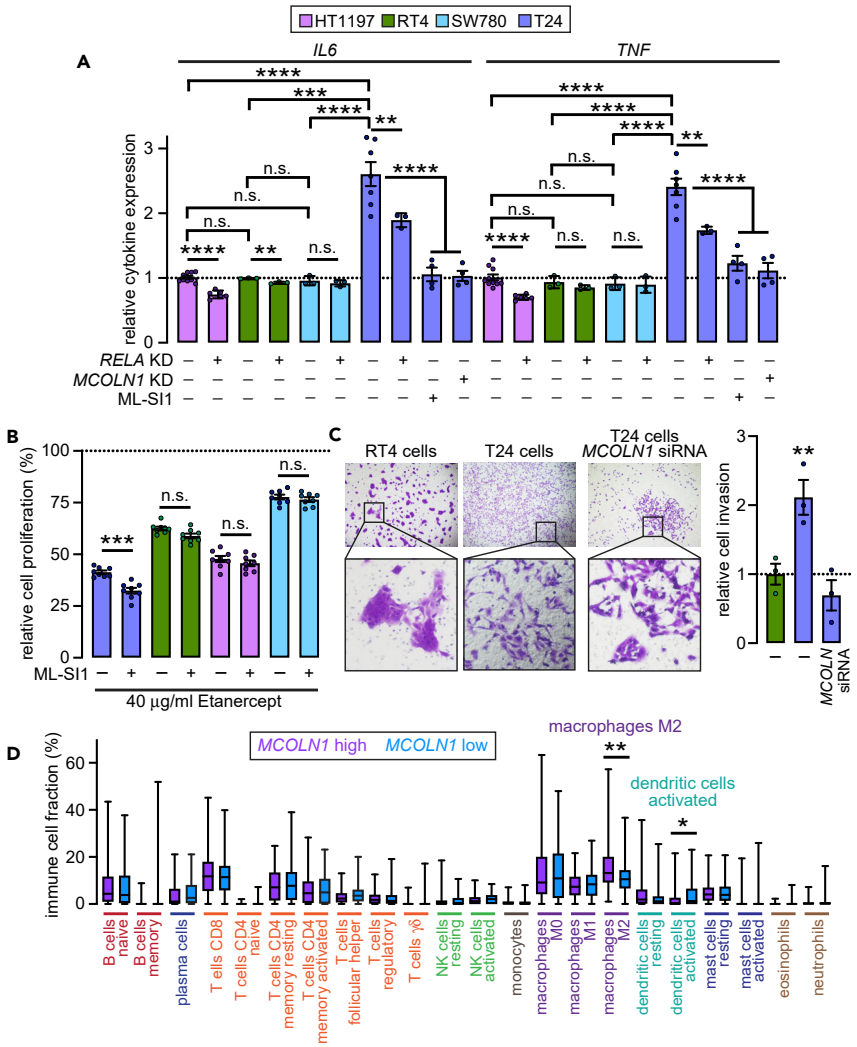

Figure 6. TRPML1 is required for cytokine gene expression in T24, but not HT1197, RT4, SW780, or 5637 bladder cancer cells

(A) Bar graph showing relative cytokine expression in the indicated cell lines treated as described. All values were normalized to the HT1197 mean. Circles represent independent biological repeats and the values shown represent mean ± SEM; **, $p < 0.01$, ***, $p < 0.001$, ****, $p < 0.0001$, t-tests with Bonferroni corrections in case of samples used in multiple pairwise comparisons. Concentrations, 50 nM *RELA* siRNA, 200 nM *MCOLN1* siRNA, and 10 µM ML-SI1.

(B) Bar graph showing relative cell numbers in response to 40 µg/mL etanercept with or without ML-SI1 as indicated at the bottom. All values were normalized to the cell numbers obtained in the absence of etanercept. Circles represent independent biological repeats and the values shown represent mean ± SEM; ***, $p < 0.001$, t test.

(C) *Left*, representative images of crystal violet stained cells from the indicated type in Matrigel. Images in the bottom row are magnifications of the regions depicted by boxes shown in the top row. T24 cells were treated with control siRNA or 200 nM *MCOLN1* siRNA. *Right*, bar graph showing the number of invading cells relative to the RT4 mean. Circles represent independent biological repeats and the values shown represent mean ± SEM; **, $p < 0.01$, ANOVA.

(D) Relative fractions of the indicated immune cell types in BLCA tumors sorted on the basis of *MCOLN1* expression (FPKM values). Fractions of immune cells were determined using CIBERSORT. *, FDR <0.05, **, FDR <0.01, Wilcoxon ranked test followed by two-stage step-up method of Benjamini, Krieger, and Yakutieli. Abbreviations: n.s., not significant.

The requirement for TRPML1 in maintaining the localization and signaling competency of $HRAS^{G12V}$ (Jung et al., 2019) raised the possibility that bladder cancer cells lacking p53 would be highly suitable for the subsequent appearance of *HRAS* mutations. In support of this notion, lentiviral transduction of $HRAS^{G12V}$ into HT1197, RT4, and 5637 led to slight increases in rates of proliferation and the acquisition of *de novo*

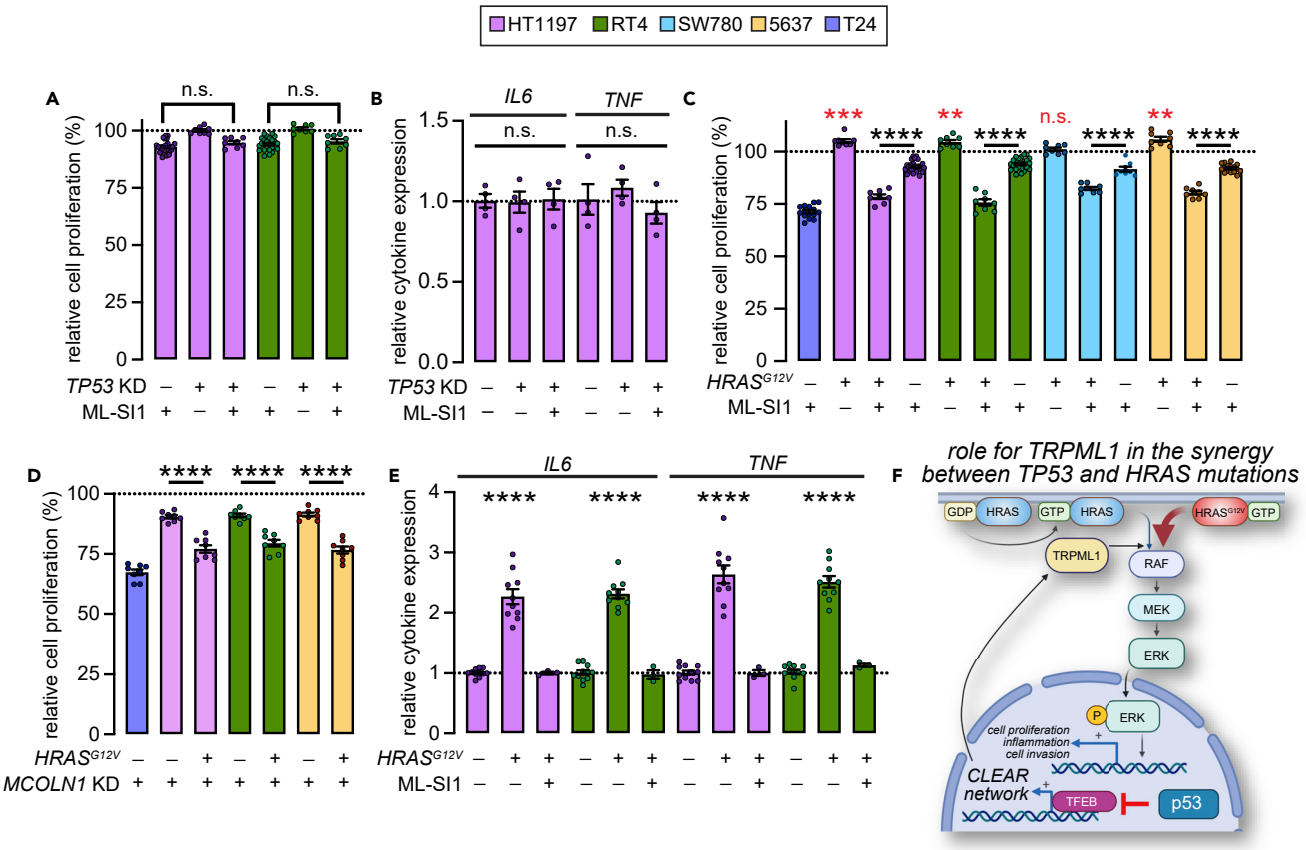

Figure 7. TRPML1 is necessary but not sufficient for cell proliferation and inflammation in bladder cancer cells

(A, C, and D) Bar graphs showing relative cell numbers in the indicated lines exposed to the conditions described below the graphs. In (A) and (C), values were normalized to HT1197 treated with DMSO alone. In (D), values were normalized to HT1197 treated with control siRNA. Circles represent independent biological repeats and the values shown represent mean ± SEM; black ****, $p < 0.0001$, t-tests; red **, $p < 0.01$, ANOVA; red, ***, $p < 0.001$, ANOVA.

(B and E) Bar graphs showing relative cytokine expression in the indicated cell lines treated as described. All values were normalized to the mean in DMSO-treated HT1197 cells. Circles represent independent biological repeats and the values shown represent mean ± SEM; ****, $p < 0.0001$, ANOVA.

(F) Schematic showing that TRPML1 is necessary for $HRAS^{G12V}$–MEK–ERK signaling. Therefore, increased *MCOLN1* expression in the absence of p53 permits MAPK-driven cell proliferation and inflammation. Concentrations, 75 nM *TP53* siRNA, 200 nM *MCOLN1* siRNA, and 10 μM ML-SI1. Abbreviation: n.s., not significant.

sensitivity toward TRPML1 inhibition or *MCOLN1* knockdown (Figures 7C and 7D, respectively). These data indicate that oncogenic *HRAS* instilled the requirement for TRPML1 function in bladder cancer cells. Ectopic $HRAS^{G12V}$ also induced a >2-fold increase in *IL6* and *TNF* transcription (Figures 7E and S7A). Indicating that cytokine expression in $HRAS^{G12V}$-expressing cells was driven by the MEK-ERK pathway, inhibition of MEK1/2 using the highly selective drug, U0126 (MEKi) (Duncia et al., 1998), attenuated expression of both *IL6* and *TNF* in T24 cells (Figure S7B). Cytokine expression driven by $HRAS^{G12V}$ was also abolished by ML-SI1 (Figure 7E). Taken together these data indicate that increased *MCOLN1* expression after the loss of p53 has a necessary role of $HRAS^{G12V}$-driven cell proliferation and inflammation but is not sufficient for either in the absence of $HRAS^{G12V}$.

DISCUSSION

p53 has a necessary and sufficient role in repressing *MCOLN1* in the urothelium

In this study, we provide multiple lines of evidence that point to a necessary and sufficient role for p53 in the regulation of *MCOLN1* expression in both malignant and healthy urothelial cells. First, in TCGA data sets, we found that *MCOLN1* was upregulated in primary BLCA tumors harboring *TP53* mutations that are predicted to ablate the transactivation function of p53. In tumors that were either wild type for *TP53* or harbored mutations in the regions of p53 that do not bind DNA, *MCOLN1* expression remained

unchanged. Another way to frame these findings is that increased *MCOLN1* expression in BLCA speaks to the preponderance of transactivation-deficient p53 mutations in this disease. Second, ectopic knockdown of *TP53* in either healthy urothelial cells or bladder cancer lines was sufficient for augmenting *MCOLN1* expression. The *MCOLN1* paralogs, *MCOLN2* and *MCOLN3*, were not as responsive to *TP53* knockdown, which suggests an element of selectivity in the relationship between p53 and the mucolipin genes. Third, we found that forced stabilization of the p53 by application of nutlin led to the repression of *MCOLN1* in both bladder cancer and healthy urothelial cells.

In agreement with prior reports that oncogenic HRAS-driven MEK-ERK signaling mediates p53 degradation via Mdm2 (Ries et al., 2000), we found that ectopic expression of $HRAS^{G12V}$ in bladder cancer cells lowered p53 abundance. These data suggest that p53 could be an intermediary in the induction of *MCOLN1* by activated HRAS (Jung et al., 2019). Given that TRPML1 ensures the transduction of signals from $HRAS^{G12V}$ to MEK–ERK (Figure 7F) (Jung et al., 2019), the relationship between activated HRAS, p53, and TRPML1 we describe is inherently protumorigenic. Although additional studies will be needed for understanding of the mechanisms by which p53 represses *MCOLN1*, the finding that *TFEB* knockdown prevented the induction of *MCOLN1* in the constitutive absence or acute knockdown of *TP53* hints at the involvement of TFEB (Figure 7F). However, *TFEB*, *TFE3,* or *MITF* do not belong to the list of p53 transcriptional targets (Allen et al., 2014). Therefore, it is likely that p53 represses the TFEB-*MCOLN1* axis indirectly—for instance, by influencing nucleocytoplasmic transport of TFEB. Reports of constitutively nuclear TFEB upon the loss of p53 in certain cancers (Zhang et al., 2017) agree with this idea. It is also noteworthy that in normal mouse fibroblasts exposed to DNA-damaging agents, p53 activates, rather than represses, TFEB/TFE3 (Brady et al., 2018). Therefore, the qualitative relationship between p53 and endolysosomal biogenesis could also depend on the cell and tissue type under observation.

TRPML1 supports oncogene-induced proliferation in p53-deficient bladder cancer cells

Given that *TP53* mutations are amongst the earliest events in bladder cancer (Gerstung et al., 2020), our data raise the possibility that elevated expression of *MCOLN1* could be occurring early in the trajectory to malignancy. These transcription changes, in turn, would increase the probability that TRPML1-dependent oncogenic pathways are subsequently activated in those cells. In agreement, our bioinformatic analyses revealed that *MCOLN1* and gene sets related to cell proliferation are concurrently induced in $TP53^{mut}$ BLCA tumors. Furthermore, in the p53-deficient and $HRAS^{G12V}$-positive T24 bladder cancer cells, inhibition of TRPML1 led to decreased rate of proliferation. The antiproliferative effects of TRPML1-inhibition results from an increase in the fraction of cells in the G_0/G_1 phase of the cell cycle and corresponding decreases in the fractions of cells in S and G2/M phases. These data agree with G_1 arrest being an outcome of MEK-ERK inhibition in RAS-transformed cancer cells (Chambard et al., 2007; Vasjari et al., 2019; Yamamoto et al., 2006). Because ML-SI1 slowed the progression of cancer cells through the cell cycle rather than inducing cell death, simultaneous application of the drug with the cytotoxic agent, cisplatin, led to a purely additive decline of T24 cell number.

Although *TP53* knockdown in RT4, HT1197, 5637, and SW780 cells increased *MCOLN1* expression, these alterations were not sufficient to accelerate cell proliferation. These data agree with the general understanding that loss of p53 is not in and of itself sufficient to initiate neoplasia but rather predisposes cells toward accumulating oncogenic mutations (Schwitalla et al., 2013). Thus, it is possible that the induction of oncogenic signaling would be more favorable in cells lacking p53 owing to attendant the elevation in *MCOLN1* expression. In agreement, introduction of $HRAS^{G12V}$ into HT1197, RT4, SW780, and 5637 cells was sufficient to confer upon those cells a requirement for functional TRPML1. Therefore, inhibition of TRPML1 or *MCOLN1* knockdown had a greater cytostatic effect on those cell lines after the ectopic expression of $HRAS^{G12V}$. These data suggest that *MCOLN1* induction, although not tumorigenic *per se*, sets the stage for oncogenic mutations that require higher TRPML1 abundance. Because TRPML1 recycles and maintains plasma membrane cholesterol (Jung et al., 2019), any signaling axis that is dependent on surface cholesterol would in principle be sensitive to TRPML1 inhibition. If so, increased *MCOLN1* expression after the loss of p53 would favor proliferation driven by several oncogenic pathways.

TRPML1 supports oncogene-induced inflammation in p53-deficient bladder cancer cells

Consistent with reports that loss of p53 triggers inflammation (Schwitalla et al., 2013), gene sets related to inflammation were upregulated in $TP53^{mut}$ BLCA tumors. Likewise, *IL6* and *TNF* mRNA were significantly higher in T24 than in RT4 or HT1197 cells. Because endolysosomal proteins such as TRPML1 are needed

for NF-κB-dependent cytokine production (El-Houjeiri et al., 2019; Sun et al., 2015; Visvikis et al., 2014; Wong et al., 2017), *MCOLN1* knockdown or TRPML1 inhibition ablated the induction of cytokines. As was the case with rates of cell proliferation, increased *MCOLN1* expression after *TP53* knockdown was not sufficient to augment cytokine gene expression. Rather, this requirement for TRPML1 also depended on the presence of activated HRAS, which drove *IL6* and *TNF* expression via MEK as an intermediary.

What might be the consequences of cytokine gene expression to the cancer cells? Prior studies have shown that TNFα can promote the proliferation of malignant cells (Gakis, 2014; Ham et al., 2016; Michaud, 2007; Wang et al., 2014; Zhu et al., 2014). In agreement, we found that application of the TNFα inhibitor, etanercept, diminished the proliferation of T24 cells to a significantly extent than did RT4, HT1197, and SW780 cells. Furthermore, the effects of etanercept on T24 cell number were enhanced by ML-SI1—a phenotype that was not observed in RT4, HT1197, and SW780 cells. TNFα has also been reported to promote cancer cell invasion (Rossi et al., 2018; Wu and Zhou, 2010; Zhu et al., 2014). In concordance with the elevation in *TNF* expression, T24 cells were significantly more invasive than were RT4 or HT1197 cells. *MCOLN1* knockdown mitigated the invasiveness of T24 cells, which agrees with TRPML1 being needed for *TNF* expression. IL6 is secreted by primary cancer cells and interacting stromal entities such as fibroblasts and compels TAMs into the anti-inflammatory, M2 state (Caetano et al., 2016; Chen et al., 2018; Cho et al., 2018; Fu et al., 2017; Mantovani et al., 2017). In agreement with our finding that TRPML1 is needed for augmented *IL6* expression, BLCA tumors with higher *MCOLN1* expression exhibited significantly greater density of M2 macrophages. Given that M2 TAMs discourage the infiltration of antitumorigenic T lymphocytes (Mantovani et al., 2017), our data raise the possibility that higher *MCOLN1* expression is predictive of an immune-cold tumor microenvironment, and thus, poor patient prognosis (Gardner and Ruffell, 2016; Gu-Trantien et al., 2013). Future studies could evaluate whether the simultaneous application of TRPML1 inhibitor and checkpoint blockers enhance the efficacy of immunotherapy.

Limitations of the study

Despite detecting an inverse relationship between p53 and *MCOLN1* expression in several transformed and normal urothelial cells, we found that the 5637 bladder cancer cells did not exhibit constitutive overexpression of *MCOLN1* despite harboring a missense mutation in the DNA-binding domain of p53 ($p53^{R280T}$). Given that p53 abundance was higher in 5637 cells than in those with wild-type alleles of *TP53*, it is possible that compensatory upregulation of p53 abundance in 5637 cells results in partial restoration of function. Indeed, siRNA-mediated knockdown of *TP53* in 5637 cells augmented *MCOLN1* expression. These data indicate that in the case of cancer cells with missense LOF mutations in p53, compensatory pathways may preclude the upregulation of *MCOLN1* expression and potentially limit the efficacy of TRPML1 inhibition. We also note that upon exposure to DNA damaging agents, p53 has been shown to activate, rather than repress, the TFEB/TFE3 transcriptional axis in normal mouse fibroblasts activates (Brady et al., 2018). Therefore, the qualitative relationship between p53 and TFEB/TFE3 targets such as TRPML1 could be a function of the cell and tissue type under observation. Finally, the relationship between *MCOLN1* expression and the immune-cold tumor microenvironment, as detected in the TCGA BLCA datasets, would need to be experimentally evaluated in tumors before targeting TRPML1 to augment immunotherapy.

STAR★METHODS

Detailed methods are provided in the online version of this paper and include the following:

- KEY RESOURCES TABLE
- RESOURCE AVAILABILITY
  - Lead contact
  - Materials availability
  - Data and code availability
- EXPERIMENTAL MODEL AND SUBJECT DETAILS
  - Cell lines and primary cultures
- METHOD DETAILS
  - Bioinformatic analyses
  - Cell culture
  - Gene knockdown by RNA interference
  - Western blotting

- Lentiviral transduction
- Analyses of cell proliferation
- Gene expression analysis
- Analyses of cell cycle
- Cell invasion assay

- QUANTIFICATION AND STATISTICAL ANALYSIS

SUPPLEMENTAL INFORMATION

Supplemental information can be found online at https://doi.org/10.1016/j.isci.2021.102701.

ACKNOWLEDGMENTS

We thank the Center for Advanced Microscopy, Department of Integrative Biology & Pharmacology at McGovern Medical School for the use of microscopes and cameras. We are grateful to Drs. Guangwei Du and Dung-Fang Lee for helpful comments on the manuscript. This work was supported by the NIH grants, RF1AG068076, R21AG061646, and R21AG067414 (all to K.V.). J.J. was supported by Korea Basic Science Institute (National research Facilities and Equipment Center) grant funded by the Ministry of Education (2019R1A6C1010044).

AUTHOR CONTRIBUTIONS

K.V. conducted the bioinformatic analyses. J.J., H.L., and S.A.C. performed the described experiments. H.L. and C.D. analyzed cell proliferation. H.L. and J.F.H. generated and provided key reagents. K.V. wrote the manuscript with input from other authors.

DECLARATION OF INTERESTS

The authors declare no competing interests.

Received: July 31, 2020
Revised: March 10, 2021
Accepted: June 7, 2021
Published: July 23, 2021

REFERENCES

Allen, M.A., Andrysik, Z., Dengler, V.L., Mellert, H.S., Guarnieri, A., Freeman, J.A., Sullivan, K.D., Galbraith, M.D., Luo, X., Kraus, W.L., et al. (2014). Global analysis of p53-regulated transcription identifies its direct targets and unexpected regulatory mechanisms. Elife *3*, e02200.

Argani, P. (2015). MiT family translocation renal cell carcinoma. Semin. Diagn. Pathol. *32*, 103–113.

Blessing, A.M., Rajapakshe, K., Reddy Bollu, L., Shi, Y., White, M.A., Pham, A.H., Lin, C., Jonsson, P., Cortes, C.J., Cheung, E., et al. (2017). Transcriptional regulation of core autophagy and lysosomal genes by the androgen receptor promotes prostate cancer progression. Autophagy *13*, 506–521.

Bouaoun, L., Sonkin, D., Ardin, M., Hollstein, M., Byrnes, G., Zavadil, J., and Olivier, M. (2016). TP53 variations in human cancers: new lessons from the IARC TP53 database and genomics data. Hum. Mutat. *37*, 865–876.

Brady, O.A., Jeong, E., Martina, J.A., Pirooznia, M., Tunc, I., and Puertollano, R. (2018). The transcription factors TFE3 and TFEB amplify p53 dependent transcriptional programs in response to DNA damage. Elife *7*, e40856.

Bubeník, J., Baresová, M., Viklický, V., Jakoubková, J., Sainerová, H., and Donner, J. (1973). Established cell line of urinary bladder carcinoma (T24) containing tumour-specific antigen. Int. J. Cancer *11*, 765–773.

Caetano, M.S., Zhang, H., Cumpian, A.M., Gong, L., Unver, N., Ostrin, E.J., Daliri, S., Chang, S.H., Ochoa, C.E., Hanash, S., et al. (2016). IL6 blockade reprograms the lung tumor microenvironment to limit the development and progression of K-ras-Mutant lung cancer. Cancer Res. *76*, 3189–3199.

Calcagni, A., Kors, L., Verschuren, E., De Cegli, R., Zampelli, N., Nusco, E., Confalonieri, S., Bertalot, G., Pece, S., Settembre, C., et al. (2016). Modelling TFE renal cell carcinoma in mice reveals a critical role of WNT signaling. Elife *5*, 1–26.

Cancer Genome Atlas Research Network (2014). Comprehensive molecular characterization of urothelial bladder carcinoma. Nature *507*, 315–322.

Chambard, J.-C., Lefloch, R., Pouysségur, J., and Lenormand, P. (2007). ERK implication in cell cycle regulation. Biochim. Biophys. Acta *1773*, 1299–1310.

Chen, L., Wang, S., Wang, Y., Zhang, W., Ma, K., Hu, C., Zhu, H., Liang, S., Liu, M., and Xu, N. (2018). IL-6 influences the polarization of macrophages and the formation and growth of colorectal tumor. Oncotarget *9*, 17443–17454.

Chiang, C.-F., Chao, T.-T., Su, Y.-F., Hsu, C.-C., Chien, C.-Y., Chiu, K.-C., Shiah, S.-G., Lee, C.-H., Liu, S.-Y., and Shieh, Y.-S. (2017). Metformin-treated cancer cells modulate macrophage polarization through AMPK-NF-κB signaling. Oncotarget *8*, 20706–20718.

Cho, H., Seo, Y., Loke, K.M., Kim, S.-W., Oh, S.-M., Kim, J.-H., Soh, J., Kim, H.S., Lee, H., Kim, J., et al. (2018). Cancer-stimulated CAFs enhance monocyte differentiation and protumoral TAM activation via IL6 and GM-CSF secretion. Clin. Cancer Res. *24*, 5407–5421.

Davidson, S.M., and Vander Heiden, M.G. (2017). Critical functions of the lysosome in cancer biology. Annu. Rev. Pharmacol. Toxicol. *57*, 481–507.

Duncia, J.V., Santella, J.B., Higley, C.A., Pitts, W.J., Wityak, J., Frietze, W.E., Rankin, F.W., Sun, J.H., Earl, R.A., Tabaka, A.C., et al. (1998). MEK inhibitors: the chemistry and biological activity of U0126, its analogs, and cyclization products. Bioorg. Med. Chem. Lett. *8*, 2839–2844.

El-Houjeiri, L., Possik, E., Vijayaraghavan, T., Paquette, M., Martina, J.A., Kazan, J.M., Ma, E.H., Jones, R., Blanchette, P., Puertollano, R., et al. (2019). The transcription factors TFEB and TFE3 link the FLCN-AMPK signaling Axis to innate immune response and pathogen resistance. Cell Rep *26*, 3613–3628.e6.

Fogh, J. (1978). Cultivation, characterization, and identification of human tumor cells with emphasis on kidney, testis, and bladder tumors. Natl. Cancer Inst. Monogr. 5–9.

Fu, X.-L., Duan, W., Su, C.-Y., Mao, F.-Y., Lv, Y.-P., Teng, Y.-S., Yu, P.-W., Zhuang, Y., and Zhao, Y.-L. (2017). Interleukin 6 induces M2 macrophage differentiation by STAT3 activation that correlates with gastric cancer progression. Cancer Immunol. Immunother. *66*, 1597–1608.

Gakis, G. (2014). The role of inflammation in bladder cancer. In Advances in Experimental Medicine and Biology, pp. 183–196.

Gardner, A., and Ruffell, B. (2016). Dendritic cells and cancer immunity. Trends Immunol. *37*, 855–865.

Gerstung, M., Jolly, C., Leshchiner, I., Dentro, S.C., Gonzalez, S., Rosebrock, D., Mitchell, T.J., Rubanova, Y., Anur, P., Yu, K., et al. (2020). The evolutionary history of 2,658 cancers. Nature *578*, 122–128.

Gu-Trantien, C., Loi, S., Garaud, S., Equeter, C., Libin, M., de Wind, A., Ravoet, M., Le Buanec, H., Sibille, C., Manfouo-Foutsop, G., et al. (2013). CD4+ follicular helper T cell infiltration predicts breast cancer survival. J. Clin. Invest. *123*, 2873–2892.

Ham, B., Fernandez, M.C., D'Costa, Z., and Brodt, P. (2016). The diverse roles of the TNF axis in cancer progression and metastasis. Trends Cancer Res. *11*, 1–27.

Hu, Z.D., Yan, J., Cao, K.Y., Yin, Z.Q., Xin, W.W., and Zhang, M.F. (2019). MCOLN1 promotes proliferation and predicts poor survival of patients with pancreatic ductal adenocarcinoma. Dis. Markers *2019*, 9436047.

Jung, J., and Venkatachalam, K. (2019). TRPML1 and RAS-driven cancers–exploring a link with great therapeutic potential. Channels *13*, 374–381.

Jung, J., Cho, K., Naji, A.K., Clemons, K.N., Wong, C.O., Villanueva, M., Gregory, S., Karagas, N.E., Tan, L., Liang, H., et al. (2019). HRAS-driven cancer cells are vulnerable to TRPML1 inhibition. EMBO Rep. *20*, e46685.

Karacsonyi, C., Miguel, A.S., and Puertollano, R. (2007). Mucolipin-2 localizes to the arf6-associated pathway and regulates recycling of GPI-APs. Traffic *8*, 1404–1414.

Kasitinon, S.Y., Eskiocak, U., Martin, M., Bezwada, D., Khivansara, V., Tasdogan, A., Zhao, Z., Mathews, T., Aurora, A.B., and Morrison, S.J. (2019). TRPML1 promotes protein homeostasis in melanoma cells by negatively regulating MAPK and mTORC1 signaling. Cell Rep. *28*, 2293–2305.e9.

Kauffman, E.C., Ricketts, C.J., Rais-Bahrami, S., Yang, Y., Merino, M.J., Bottaro, D.P., Srinivasan, R., and Linehan, W.M. (2014). Molecular genetics and cellular features of TFE3 and TFEB fusion kidney cancers. Nat. Rev. Urol. *11*, 465–475.

Kundu, S.T., Grzeskowiak, C.L., Fradette, J.J., Gibson, L.A., Rodriguez, L.B., Creighton, C.J., Scott, K.L., and Gibbons, D.L. (2018). TMEM106B drives lung cancer metastasis by inducing TFEB-dependent lysosome synthesis and secretion of cathepsins. Nat. Commun. *9*, 2731.

Li, S., Song, Y., Quach, C., Guo, H., Jang, G.-B., Maazi, H., Zhao, S., Sands, N.A., Liu, Q., In, G.K., et al. (2019). Transcriptional regulation of autophagy-lysosomal function in BRAF-driven melanoma progression and chemoresistance. Nat. Commun. *10*, 1693.

Mantovani, A., Marchesi, F., Malesci, A., Laghi, L., and Allavena, P. (2017). Tumour-associated macrophages as treatment targets in oncology. Nat. Rev. Clin. Oncol. *14*, 399–416.

Martina, J.A., Chen, Y., Gucek, M., and Puertollano, R. (2012). MTORC1 functions as a transcriptional regulator of autophagy by preventing nuclear transport of TFEB. Autophagy *8*, 903–914.

Martina, J.A., Diab, H.I., Lishu, L., Jeong-A., L., Patange, S., Raben, N., and Puertollano, R. (2014). The nutrient-responsive transcription factor TFE3 promotes autophagy, lysosomal biogenesis, and clearance of cellular debris. Sci. Signal. *7*, ra9.

Medina, D.L., Di Paola, S., Peluso, I., Armani, A., De Stefani, D., Venditti, R., Montefusco, S., Scotto-Rosato, A., Prezioso, C., Forrester, A., et al. (2015). Lysosomal calcium signalling regulates autophagy through calcineurin and TFEB. Nat. Cell Biol. *17*, 288–299.

Michaud, D.S. (2007). Chronic inflammation and bladder cancer. Urol. Oncol. Semin. Orig. Investig. *25*, 260–268.

Newman, A.M., Liu, C.L., Green, M.R., Gentles, A.J., Feng, W., Xu, Y., Hoang, C.D., Diehn, M., and Alizadeh, A.A. (2015). Robust enumeration of cell subsets from tissue expression profiles. Nat. Methods *12*, 453–457.

Nolan, G.P., Ghosh, S., Liou, H.C., Tempst, P., and Baltimore, D. (1991). DNA binding and IκB inhibition of the cloned p65 subunit of NF-κB, a rel-related polypeptide. Cell *64*, 961–969.

Di Palma, F., Belyantseva, I.A., Kim, H.J., Vogt, T.F., Kachar, B., and Noben-Trauth, K. (2002). Mutations in Mcoln3 associated with deafness and pigmentation defects in varitint-waddler (Va) mice. Proc. Natl. Acad. Sci. *99*, 14994–14999.

Palmieri, M., Impey, S., Kang, H., di Ronza, A., Pelz, C., Sardiello, M., and Ballabio, A. (2011). Characterization of the CLEAR network reveals an integrated control of cellular clearance pathways. Hum. Mol. Genet. *20*, 3852–3866.

Palmieri, M., Pal, R., Nelvagal, H.R., Lotfi, P., Stinnett, G.R., Seymour, M.L., Chaudhury, A., Bajaj, L., Bondar, V.V., Bremner, L., et al. (2017). mTORC1-independent TFEB activation via Akt inhibition promotes cellular clearance in neurodegenerative storage diseases. Nat. Commun. *8*, 14338.

Perera, R.M., Stoykova, S., Nicolay, B.N., Ross, K.N., Fitamant, J., Boukhali, M., Lengrand, J., Deshpande, V., Selig, M.K., Ferrone, C.R., et al. (2015). Transcriptional control of autophagy-lysosome function drives pancreatic cancer metabolism. Nature *524*, 361–365.

Perera, R.M., Di Malta, C., and Ballabio, A. (2019). MiT/TFE family of transcription factors, lysosomes, and cancer. Annu. Rev. Cancer Biol. *3*, 203–222.

Ploper, D., Taelman, V.F., Robert, L., Perez, B.S., Titz, B., Chen, H.-W., Graeber, T.G., von Euw, E., Ribas, A., and De Robertis, E.M. (2015). MITF drives endolysosomal biogenesis and potentiates Wnt signaling in melanoma cells. Proc. Natl. Acad. Sci. *112*, E420–E429.

Rasheed, S., Gardner, M.B., Rongey, R.W., Nelson-Rees, W.A., and Arnstein, P. (1977). Human bladder carcinoma: characterization of two new tumor cell lines and search for tumor viruses. J. Natl. Cancer Inst. *58*, 881–890.

Ries, S., Biederer, C., Woods, D., Shifman, O., Shirasawa, S., Sasazuki, T., McMahon, M., Oren, M., and McCormick, F. (2000). Opposing effects of Ras on p53: transcriptional activation of mdm2 and induction of p19ARF. Cell *103*, 321–330.

Rigby, C.C., and Franks, L.M. (1970). A human tissue culture cell line from a transitional cell tumour of the urinary bladder: growth, chromosome pattern and ultrastructure. Br. J. Cancer *24*, 746–754.

Robertson, A.G., Kim, J., Al-Ahmadie, H., Bellmunt, J., Guo, G., Cherniack, A.D., Hinoue, T., Laird, P.W., Hoadley, K.A., Akbani, R., et al. (2017). Comprehensive molecular characterization of muscle-invasive bladder cancer. Cell *171*, 540–556.e25.

Robinson, M.D., McCarthy, D.J., and Smyth, G.K. (2010). edgeR: a Bioconductor package for differential expression analysis of digital gene expression data. Bioinformatics *26*, 139–140.

Roczniak-Ferguson, A., Petit, C.S., Froehlich, F., Qian, S., Ky, J., Angarola, B., Walther, T.C., and Ferguson, S.M. (2012). The transcription factor TFEB links mTORC1 signaling to transcriptional control of lysosome homeostasis. Sci. Signal. *5*, ra42.

Rossi, S., Cordella, M., Tabolacci, C., Nassa, G., D'Arcangelo, D., Senatore, C., Pagnotto, P., Magliozzi, R., Salvati, A., Weisz, A., et al. (2018). TNF-alpha and metalloproteases as key players in melanoma cells aggressiveness. J. Exp. Clin. Cancer Res. *37*, 326.

Samie, M., Wang, X., Zhang, X., Goschka, A., Li, X., Cheng, X., Gregg, E., Azar, M., Zhuo, Y., Garrity, A.G., et al. (2013). A TRP channel in the lysosome regulates large particle phagocytosis via focal exocytosis. Dev. Cell *26*, 511–524.

Sardiello, M., Palmieri, M., di Ronza, A., Medina, D.L., Valenza, M., Gennarino, V.A., Di Malta, C., Donaudy, F., Embrione, V., Polishchuk, R.S., et al. (2009). A gene network regulating lysosomal biogenesis and function. Science *325*, 473–477.

Schindelin, J., Arganda-Carreras, I., Frise, E., Kaynig, V., Longair, M., Pietzsch, T., Preibisch, S., Rueden, C., Saalfeld, S., Schmid, B., et al. (2012). Fiji: an open-source platform for biological-image analysis. Nat. Methods *9*, 676–682.

Schwitalla, S., Ziegler, P.K., Horst, D., Becker, V., Kerle, I., Begus-Nahrmann, Y., Lechel, A., Rudolph, K.L., Langer, R., Slotta-Huspenina, J., et al. (2013). Loss of p53 in enterocytes generates an inflammatory microenvironment enabling invasion and lymph node metastasis of carcinogen-induced colorectal tumors. Cancer Cell *23*, 93–106.

Settembre, C., Di Malta, C., Polito, V.A., Arencibia, M.G., Vetrini, F., Erdin, S., Erdin, S.U., Huynh, T., Medina, D., Colella, P., et al. (2011). TFEB links autophagy to lysosomal biogenesis. Science *332*, 1429–1433.

Settembre, C., Zoncu, R., Medina, D.L., Vetrini, F., Erdin, S., Erdin, S., Huynh, T., Ferron, M., Karsenty, G., Vellard, M.C., et al. (2012). A lysosome-to-nucleus signalling mechanism senses and regulates the lysosome via mTOR and TFEB. EMBO J. *31*, 1095–1108.

Shannon, C.E. (1948). A mathematical theory of communication. Bell Syst. Tech. J. *27*, 379–423.

Shannon, P., Markiel, A., Ozier, O., Baliga, N.S., Wang, J.T., Ramage, D., Amin, N., Schwikowski, B., and Ideker, T. (2003). Cytoscape: a software environment for integrated models of biomolecular interaction networks. Genome Res. *13*, 2498–2504.

Subramanian, A., Tamayo, P., Mootha, V.K., Mukherjee, S., Ebert, B.L., Gillette, M.A., Paulovich, A., Pomeroy, S.L., Golub, T.R., Lander, E.S., et al. (2005). Gene set enrichment analysis: a knowledge-based approach for interpreting genome-wide expression profiles. Proc. Natl. Acad. Sci. U S A *102*, 15545–15550.

Suffredini, A.F., Reda, D., Banks, S.M., Tropea, M., Agosti, J.M., and Miller, R. (1995). Effects of recombinant dimeric TNF receptor on human inflammatory responses following intravenous endotoxin administration. J. Immunol. *155*, 5038–5045.

Sun, L., Hua, Y., Vergarajauregui, S., Diab, H.I., and Puertollano, R. (2015). Novel role of TRPML2 in the regulation of the innate immune response. J. Immunol. *195*, 4922–4932.

Tasdemir, E., Chiara Maiuri, M., Morselli, E., Criollo, A., D'Amelio, M., Djavaheri-Mergny, M., Cecconi, F., Tavernarakis, N., and Kroemer, G. (2008a). A dual role of p53 in the control of autophagy. Autophagy *4*, 810–814.

Tasdemir, E., Maiuri, M.C., Galluzzi, L., Vitale, I., Djavaheri-Mergny, M., D'Amelio, M., Criollo, A., Morselli, E., Zhu, C., Harper, F., et al. (2008b). Regulation of autophagy by cytoplasmic p53. Nat. Cell Biol. *10*, 676–687.

Vasjari, L., Bresan, S., Biskup, C., Pai, G., and Rubio, I. (2019). Ras signals principally via Erk in G1 but cooperates with PI3K/Akt for Cyclin D induction and S-phase entry. Cell Cycle *18*, 204–225.

Vassilev, L.T., Vu, B.T., Graves, B., Carvajal, D., Podlaski, F., Filipovic, Z., Kong, N., Kammlott, U., Lukacs, C., Klein, C., et al. (2004). In vivo activation of the p53 pathway by small-molecule antagonists of MDM2. Science *303*, 844–848.

Visvikis, O., Ihuegbu, N., Labed, S.A., Luhachack, L.G., Alves, A.-M.F., Wollenberg, A.C., Stuart, L.M., Stormo, G.D., and Irazoqui, J.E. (2014). Innate host defense requires TFEB-mediated transcription of cytoprotective and antimicrobial genes. Immunity *40*, 896–909.

Wang, D.J., Ratnam, N.M., Byrd, J.C., and Guttridge, D.C. (2014). NF-κB functions in tumor initiation by suppressing the surveillance of both innate and adaptive immune cells. Cell Rep. *9*, 90–103.

Wang, W., Gao, Q., Yang, M., Zhang, X., Yu, L., Lawas, M., Li, X., Bryant-Genevier, M., Southall, N.T., Marugan, J., et al. (2015). Up-regulation of lysosomal TRPML1 channels is essential for lysosomal adaptation to nutrient starvation. Proc. Natl. Acad. Sci. *112*, E1373–E1381.

Wong, C.-O., Gregory, S., Hu, H., Chao, Y., Sepúlveda, V.E., He, Y., Li-Kroeger, D., Goldman, W.E., Bellen, H.J., and Venkatachalam, K. (2017). Lysosomal degradation is required for sustained phagocytosis of bacteria by macrophages. Cell Host Microbe *21*, 719–730.e6.

Wu, Y., and Zhou, B.P. (2010). TNF-α/NF-κB/Snail pathway in cancer cell migration and invasion. Br. J. Cancer *102*, 639–644.

Xu, H., and Ren, D. (2015). Lysosomal physiology. Annu. Rev. Physiol. *77*, 57–80.

Xu, J., Zeng, J.Q., Wan, G., Hu, G.B., Yan, H., and Ma, L.X. (2009). Construction of siRNA/miRNA expression vectors based on a one-step PCR process. BMC Biotechnol. *9*, 53.

Xu, M., Almasi, S., Yang, Y., Yan, C., Sterea, A.M., Rizvi Syeda, A.K., Shen, B., Richard Derek, C., Huang, P., Gujar, S., et al. (2019). The lysosomal TRPML1 channel regulates triple negative breast cancer development by promoting mTORC1 and purinergic signaling pathways. Cell Calcium *79*, 80–88.

Yamamoto, T., Ebisuya, M., Ashida, F., Okamoto, K., Yonehara, S., and Nishida, E. (2006). Continuous ERK activation downregulates antiproliferative genes throughout G1 phase to allow cell-cycle progression. Curr. Biol. *16*, 1171–1182.

Yin, C., Zhang, H., Liu, X., Zhang, H., Zhang, Y., Bai, X., Wang, L., Li, H., Li, X., Zhang, S., et al. (2019). Downregulated MCOLN1 attenuates the progression of non-small-cell lung cancer by inhibiting lysosome-autophagy. Cancer Manag. Res. *11*, 8607–8617.

Zhang, Z., Wang, H., Ding, Q., Xing, Y., Xu, D., Xu, Z., Zhou, T., Qian, B., Ji, C., Pan, X., et al. (2017). The tumor suppressor p53 regulates autophagosomal and lysosomal biogenesis in lung cancer cells by targeting transcription factor EB. Biomed. Pharmacother. *89*, 1055–1060.

Zhou, Y., Xia, Z., Cheng, Z., Xu, G., Yang, X., Liu, S., and Zhu, Y. (2018). Inducible microRNA-590-5p inhibits host antiviral response by targeting the soluble interleukin-6 (IL6) receptor. J. Biol. Chem. *293*, 18168–18179.

Zhu, G., Du, Q., Wang, Xi., Tang, N., She, F., and Chen, Y. (2014). TNF-α promotes gallbladder cancer cell growth and invasion through autocrine mechanisms. Int. J. Mol. Med. *33*, 1431–1440.

STAR★METHODS

KEY RESOURCES TABLE

REAGENT or RESOURCE	SOURCE	IDENTIFIER
Antibodies		
Mouse monoclonal anti-p53 antibody (DO-1)	Santa Cruz Biotechnology	Cat#: sc-126; RRID: AB_628082
Mouse monoclonal anti-β-tubulin antibody (E7)	DSHB	Cat#: E7; RRID: AB_528499
Goat anti-mouse IRDye 800CW secondary antibodies	LI-COR Biosciences	Cat#: 925-32210; RRID: AB_2687825
Mouse anti-BrdU (clone B44)	BD Biosciences	Cat#: 347580
Alexa Fluor 488 goat anti-mouse secondary antibodies	Invitrogen	Cat#: A11001
Bacterial and virus strains		
LV-HRAS^{G12V}-GFP	This paper	N/A
Chemicals, peptides, and recombinant proteins		
Nutlin-3a	Tocris	Cat#: 6075
ML-SI1 (GW-405833)	Sigma	Cat#: G1421
Cisplatin	Sigma	Cat#: PHR1624
Etanercept	Sigma	Cat#: Y0001969
U0126 (MEKi)	Sigma	Cat#: 19-147
Propidium iodide	Sigma	Cat#: 81845
Bromodeoxyuridine (BrdU)	Acros	Cat#228590010
RNAse	Sigma	Cat#: R6513
Hexadimethrine bromide	Sigma	Cat#: H9268
Crystal violet	Sigma	Cat#: C6158
Critical commercial assays		
X-treme GENE 9 DNA Transfection reagents	Roche	Cat#: 6365779001
WST-1 cell proliferation assay	Roche	Cat#: 5015944001
Cultrex® Cell Migration Assay	Trevigen	Cat#: 3465-024-K
RNeasy Mini Kit	Qiagen	Cat#: 74004
High-Capacity cDNA Reverse Transcription Kit	Applied Biosystems	Cat#: 43-688-14
SYBR Green JumpStart Taq ReadyMix	Sigma	Cat#: S4438
Experimental models: Cell lines		
Human: HT1197 cells	ATCC	RRID: CVCL_1291
Human: RT4 cells	ATCC	RRID: CVCL_0036
Human: SW780 cells	ATCC	RRID: CVCL_1728
Human: 5637 cells	ATCC	RRID: CVCL_0126
Human: T24 cells	ATCC	RRID: CVCL_0554
Human: Primary urothelial cells	ATCC	Cat#: PCS-420-010
Oligonucleotides		
MCOLN1 siRNA — 5′-CCCACATCCAGGAGTGTAA-3′	Jung et al. (2019)	N/A
TP53 siRNA — 5′-AGACTCCAGTGGTAATCTA-3′	Xu et al. (2009)	N/A

(*Continued on next page*)

Continued

REAGENT or RESOURCE	SOURCE	IDENTIFIER
RELA siRNA — 5′-GGAGTACCCTGAGGCTAT-3′	This paper	N/A
TFEB siRNA — 5′-CCGCCTGGAGATGACCAACAA-3′	Jung et al. (2019)	N/A
MISSION® siRNA Universal Negative Control (Control siRNA)	Sigma	Cat#: SIC001
GAPDH sequencing: Forward: 5′-GAAGGTGAAGGTCGGAGTC-3′ Reverse: 5′-GAAGATGGTGATGGGATTTC-3′	Jung et al. (2019)	N/A
IL6 sequencing: Forward: 5′-AGACAGCCACTCACCTCTTCAG-3′ Reverse: 5′-TTCTGCCAGTGCCTCTTTGCTG-3′	Zhou et al. (2018)	N/A
MCOLN1 sequencing: Forward: 5′-CTGGTGGTCACGGTGCAG-3′ Reverse: 5′-CTGCTCCCGCGTGTAGG -3′	Jung et al. (2019)	N/A
MCOLN2 sequencing: Forward: 5′-CGGCAGCCTTATCGTTTTCC-3′ Reverse: 5′-GCCATTGCATTTCTGACGGT-3′	Jung et al. (2019)	N/A
MCOLN3 sequencing: Forward: 5′-TCTCCTCCCGTCTGACTCTG-3′ Reverse: 5′-CAGGATCTGCCATCTCTGGG-3′	Jung et al. (2019)	N/A
RELA sequencing: Forward: 5′-TGAACCGAAACTCTGGCAGCTG-3′ Reverse: 5′-CATCAGCTTGCGAAAAGGAGCC-3′	This paper	N/A
TFEB sequencing: Forward: 5′-CCAGAAGCGAGAGCTCACAGAT-3′ Reverse: 5′-TGTGATTGTCTTTCTTCTGCCG-3′	Jung et al. (2019)	N/A
TNFA sequencing: Forward: 5′-CTCTTCTGCCTGCTGCACTTTG-3′ Reverse: 5′-ATGGGCTACAGGCTTGTCACTC-3′	Chiang et al. (2017)	N/A
Recombinant DNA		
LV-HRAS^{G12V}-GFP	This paper	N/A
Software and algorithms		
Fiji (ImageJ)	Schindelin et al. (2012)	https://imagej.net/Fiji
Prism8	Graphpad	https://www.graphpad.com/scientific-software/prism/
RStudio	RStudio	https://www.rstudio.com
EdgeR	Robinson et al. (2010)	https://bioconductor.org/packages/release/bioc/html/edgeR.html
GSEA	Subramanian et al. (2005)	https://www.gsea-msigdb.org/gsea/index.jsp
CytoScape	Shannon et al. (2003)	https://cytoscape.org
Cibersort	Newman et al. (2015)	https://cibersort.stanford.edu
Determination of Shannon information	This study	https://github.com/kvenkatachalam-lab/ung-et-al.-2021-iScience-paper

RESOURCE AVAILABILITY

Lead contact

Further information and requests for resources and reagents should be directed to and will be fulfilled by the lead contact, Kartik Venkatachalam (kartik.venkatachalam@uth.tmc.edu).

Materials availability

This study did not generate new unique reagents.

Data and code availability

All bioinformatic data used in this manuscript were obtained from TCGA as indicated in the *Method Details* and are included in the supplemental tables. No new datasets were generated in this study. The code generated during this study are available at GitHub (https://github.com/kvenkatachalam-lab/Jung-et-al.-2021-iScience-paper).

EXPERIMENTAL MODEL AND SUBJECT DETAILS

Cell lines and primary cultures

The following cancer cell lines were used in the study:

1. **HT1197 cells** (RRID: CVCL_1291).

Origin: Human bladder carcinoma cell line obtained from a 44-year-old male.

Culture media and conditions: HT1197 cells were obtained from ATCC and were cultured in DMEM high glucose media containing 2mM L-glutamine and supplemented with 10% (v/v) inactivated fetal bovine serum (FBS), penicillin-streptomycin, non-essential amino acids, and pyruvate. Cells were maintained in a 37°C incubator under 5% CO_2. We did not authenticate this cell line in our laboratory.

2. **RT4 cells** (RRID: CVCL_0036).

Origin: Human bladder carcinoma cell line obtained from a 63-year-old male.

Culture media and conditions: RT4 cells were obtained from ATCC and were cultured in DMEM high glucose media containing 2mM L-glutamine and supplemented with 10% (v/v) inactivated fetal bovine serum (FBS), penicillin-streptomycin, non-essential amino acids, and pyruvate. Cells were maintained in a 37°C incubator under 5% CO_2. We did not authenticate this cell line in our laboratory.

3. **SW780 cells** (RRID: CVCL_1728).

Origin: Human bladder carcinoma cell line obtained from an 80-year-old female.

Culture media and conditions: SW780 cells were obtained from ATCC and were cultured in DMEM high glucose media containing 2mM L-glutamine and supplemented with 10% (v/v) inactivated fetal bovine serum (FBS), penicillin-streptomycin, non-essential amino acids, and pyruvate. Cells were maintained in a 37°C incubator under 5% CO_2. We did not authenticate this cell line in our laboratory.

4. **5637 cells** (RRID: CVCL_0126).

Origin: Human bladder carcinoma cell line obtained from a 68-year-old male.

Culture media and conditions: 5637 cells were obtained from ATCC and were cultured in DMEM high glucose media containing 2mM L-glutamine and supplemented with 10% (v/v) inactivated fetal bovine serum (FBS), penicillin-streptomycin, non-essential amino acids, and pyruvate. Cells were maintained in a 37°C incubator under 5% CO_2. We did not authenticate this cell line in our laboratory.

5. **T24 cells** (RRID: CVCL_0554).

Origin: Human bladder carcinoma cell line obtained from an 82-year-old female.

Culture media and conditions: T24 cells were obtained from ATCC and were cultured in DMEM high glucose media containing 2mM L-glutamine and supplemented with 10% (v/v) inactivated fetal bovine

serum (FBS), penicillin-streptomycin, non-essential amino acids, and pyruvate. Cells were maintained in a 37°C incubator under 5% CO_2. We did not authenticate this cell line in our laboratory.

The following primary cells were used in the study:

1. **Primary urothelial cells** (ATCC PCS-420-010)

Origin: Human primary urothelial cells. Sex of the cells, which are batch specific, was not known.

Culture media and conditions: Primary urothelial cells were cultured in bladder epithelial cell basal medium (ATCC-PCS-420-032) supplemented with bladder epithelial cell growth kit (ATCC-PCS-420-042). We did not authenticate this cell line in our laboratory.

METHOD DETAILS

Bioinformatic analyses

Analyses of differential gene expression. Raw counts (CPM) from the RNA-seq analyses of BLCA tumors and matched controls were obtained from GDC (https://portal.gdc.cancer.gov). Differential expression was determined using EdgeR (Robinson et al., 2010) with FDR < 0.05 as the cutoff.

Analyses of correlation with MCOLN1. Spearman's correlation coefficients of coexpression with *MCOLN1* in BLCA were obtained from cBioPortal (https://www.cbioportal.org). FDR < 0.05 was the cutoff for determining genes that were significantly correlated with *MCOLN1*.

GSEA. GSEA was performed using the standalone GSEA_4.0.3 application downloaded from www.gsea-msigdb.org. Pre-ranked GSEA was performed using either custom gene sets or gene sets obtained from MSigDB. For the analyses, no collapse was used, and the default minimum and maximum exclusion criteria of 15 and 500, respectively.

Analyses of networks. We used CytoScape (Shannon et al., 2003) to generate networks using the results of GSEA analyses. Gene sets were nodes and extent of overlap between the sets represented edge values. Node size represented number of genes, whereas node color represented normalized enrichment score (NES) from GSEA analyses.

Determination of Shannon information. List of somatic mutations (SNPs and small INDELs) that were determined using MuTect2 variant aggregation and masking were obtained from the UCSC Xena functional genomics browser (https://xenabrowser.net/datapages/). Using a custom R script, we filtered all synonymous mutations, and genes that did not belong to the consensus list of 722 CGCs (https://cancer.sanger.ac.uk/census; Table S3). Tumors were then ranked on the basis of *MCOLN1* FPKM values. The ranked set was then partitioned into groups comprised of tumors that belonged to either the top third or the bottom third of the ranked list. Conditional probability that mutations in a gene would occur in tumors that belonged to a group was calculated using the formula:

$$P(mutation|group)$$

$$= \frac{P(tumors\ in\ the\ group).P(mutations\ in\ gene\ occur\ in\ the\ group)}{P(tumors\ in\ the\ group).P(mutations\ in\ gene\ occur\ in\ the\ group)}$$

$$+ P(tumors\ not\ in\ the\ group).P(mutations\ in\ gene\ occur\ in\ tumors\ not\ in\ the\ group)$$

Entropy associated with gene mutations occurring in a group was calculated using the formula:

$$H(mutation, group) = -P(mutation|group).\log_2 P(mutation|group) - (1 - P(mutation|group)).$$

$$\log_2(1 - P(mutation|group))$$

Shannon information was calculated using the formula:

$$I(gene, group) = H(mutation\ in\ gene, all\ tumors) - \frac{1}{3}H(mutation\ in\ gene, in\ group) - \frac{2}{3}H(mutation\ in\ gene,\ not\ in\ group)$$

For the permutation test, we first generated a null dataset comprised of information values for each gene obtained after randomly reordering the assignment of *MCOLN1* FPKM values. Default number of permutations was 1000. Nominal P-values were calculated by comparing computed information for each gene with the respective values from the null dataset using a one-sample t-test. FDR *Q* values were calculated from the nominal P-values by applying the Benjamini and Hochberg correction.

CIBERSORT analyses. Distribution of immune cell types in the BLCA tumors was determined using the online portal (https://cibersort.stanford.edu/index.php). Fractions of each immune cell type were then compared in groups of tumors sorted on the basis of *MCOLN1* FPKM values. Pairwise comparisons were made using the Mann-Whitney test, and FDR was analyzed using the two-stage step-up method of Benjamini, Krieger and Yakutieli.

Cell culture

T24, HT1197, RT4, SW780, and 5637 cell lines (all from ATCC) were cultured in DMEM high glucose media containing 2mM L-glutamine and supplemented with 10% (v/v) inactivated fetal bovine serum (FBS), penicillin-streptomycin, non-essential amino acids, pyruvate (all from Fischer Scientific). Primary urothelial cells (ATCC PCS-420-010) were cultured in bladder epithelial cell basal medium (ATCC-PCS-420-032) supplemented with bladder epithelial cell growth kit (ATCC-PCS-420-042). All of the cell lines were maintained at 37°C and 5% CO_2. For drug treatment, we added DMSO (vehicle) or the drugs directly to the cell media.

Gene knockdown by RNA interference

For siRNA transfections, cells were transfected with siRNA oligonucleotides using X-treme GENE 9 DNA Transfection reagents (Roche) following manufacturer's instructions. Subsequent analyses were performed after 2- or 5-days of siRNA treatment. The following sequences were used:

MCOLN1 — 5′-CCCACATCCAGGAGTGTAA-3′ (200 nM)

TP53 — 5′-AGACTCCAGTGGTAATCTA-3′ (75 nM)

RELA — 5′-GGAGTACCCTGAGGCTAT-3′ (50 nM)

TFEB — 5′-CCGCCTGGAGATGACCAACAA-3′ (50 nM)

Control siRNA (SIC001, Sigma-Aldrich) was used as a negative control. Concentration of control siRNA was equal to that of the specific siRNA.

Western blotting

When generating cellular extracts for Western blotting, we harvested cells in a lysis buffer containing protease inhibitors and DTT. We loaded the cell extracts onto 4–20% gradient Tri-glycine gels (Bio-Rad) for SDS–PAGE. After transfer to nitro- cellulose membranes, the blots were blocked using the Odyssey blocking buffer (LI-COR Biosciences) followed by incubation with primary antibodies and secondary antibodies described below. All blots were imaged using the Odyssey imaging platform (LI-COR Biosciences). For quantification, we determined band intensities using Fiji/ImageJ (NIH) (Schindelin et al., 2012). When probing the blots with antibodies from the same species, we stripped the blots using the NewBlotTM nitrocellulose stripping buffer as per the manufacturer's instructions (LI- COR Biosciences). All antibody incubations were performed in the Odyssey blocking buffer (LI-COR Biosciences). Primary antibodies used were mouse anti-p53 (1:2000, DO-1, Santa Cruz Biotechnology), and mouse anti-β-tubulin (1:2000, E7, DSHB). Secondary antibodies used were goat anti-mouse IRDye 800CW (LI-COR Biosciences).

Lentiviral transduction

To ectopically express HRAS^{G12V} in bladder cancer cells, we transduced cells with a *HRAS^{G12V}-GFP* lentiviral construct. Briefly, we treated cells with cell culture media containing lentivirus and 4 μg/ml of hexadimethrine bromide (Sigma) for 12 hours. After 12 hours, we removed this media and added full growth media. We incubated the cells for 48 hours before adding media with puromycin (1:5000 dilution) for selection of cells expressing *HRAS^{G12V}-GFP*.

Analyses of cell proliferation

WST-1 assay. Cells were seeded in 96-well plates at the density of 10^4 cells/well and incubated for 12 hours at 37°C (CO_2). Subsequently, fresh media containing DMSO or drugs or control or specific siRNA was applied to the cells. Cell numbers were assessed 2- or 5-days later using the WST-1 (4-(3-(4- iodophenyl)-2-(4-nitrophenyl)-2H-5-tetrazolio)-1,3-benzene disulfonate, Roche Applied Sciences) assay as per the manufacturer's protocol. Absorbance was measured using a microplate ELISA reader (Cytation 5, BioTek) at 450 nm.

Crystal violet staining. Cells were seeded in 6-well plates ($2x10^5$ cells/well), and exposed to 10 μM MLSI for the indicated durations. Cells were then fixed for 5 minutes with 4% PFA, and stained for 10 minutes with 0.5% crystal violet (Sigma) diluted in PBS. After a series of washes in plain water, plates were dried and images were captured. Subsequently, crystal violet signal from the plates was solubilized in 100 μl methanol, and absorbances of the solutions were read at 540 nm.

Gene expression analysis

When performing RT-qPCR, total RNA was extracted with RNeasy Mini Kit (Qiagen) following manufacturer's instructions. 1μg of total RNA was reverse-transcribed with High-Capacity cDNA Reverse Transcription Kit (Applied Biosystems). Real-time qPCR was performed using SYBR Green JumpStart Taq ReadyMix (Sigma) as per the manufacturer's protocol. Primers used have been described previously (Chiang et al., 2017; Jung et al., 2019; Zhou et al., 2018), and were as follows:

GAPDH:

Forward: 5'-GAAGGTGAAGGTCGGAGTC-3'

Reverse: 5'-GAAGATGGTGATGGGATTTC-3'

MCOLN1:

Forward: 5'-CTGGTGGTCACGGTGCAG-3'

Reverse: 5'-CTGCTCCCGCGTGTAGG -3'

MCOLN2:

Forward: 5'-CGGCAGCCTTATCGTTTTCC-3'

Reverse: 5'-GCCATTGCATTTCTGACGGT-3'

MCOLN3:

Forward: 5'-TCTCCTCCCGTCTGACTCTG-3'

Reverse: 5'-CAGGATCTGCCATCTCTGGG-3'

RELA:

Forward: 5'-TGAACCGAAACTCTGGCAGCTG-3'

Reverse: 5′-CATCAGCTTGCGAAAAGGAGCC-3′

TFEB:

Forward: 5′-CCAGAAGCGAGAGCTCACAGAT-3′

Reverse: 5′-TGTGATTGTCTTTCTTCTGCCG-3′

IL6:

Forward: 5′-AGACAGCCACTCACCTCTTCAG-3′

Reverse: 5′-TTCTGCCAGTGCCTCTTTGCTG-3′

TNFA:

Forward: 5′-CTCTTCTGCCTGCTGCACTTTG-3′

Reverse: 5′-ATGGGCTACAGGCTTGTCACTC-3′

Analyses of cell cycle

Number of cells in G1, S or G2/M phases of the cell cycle was determined by measuring DNA content using propidium iodide (PI) and bromodeoxyuridine (BrdU) labeling followed by flow cytometry analysis. Cells were pulsed with 10 μM BrdU for 45 minutes, harvested and fixed with 70% ice-cold ethanol overnight. Cells were washed in BrdU wash solution (0.5% Tween 20, 0.5% BSA in PBS) and resuspended in 2 N HCl for 20 minutes at room temperature. 0.1 M sodium borate was added to neutralize, and the cells were washed twice with BrdU wash solution. Cells were incubated with anti-BrdU antibody (BD 347580 mouse IgG) at room temperature for 30 minutes, washed thrice in BrdU wash solution and incubated with Alexa Fluor 488 goat anti-mouse IgG (Invitrogen) for 30 minutes at room temperature. After three washes with BrdU wash solution, the cells were treated with 100 ug/ml RNase and 25 μg/ml propidium iodide for 20 minutes at 37°C. Analyses were performed using a BD LSRFortessa instrument.

Cell invasion assay

3×10^3 cells in 100 μL serum-free DMEM were placed into the upper chamber of a 24-well Transwell insert (8 μm pore size; Trevigen) coated with 10% of Matrigel (v/v, Corning). 500 μL complete media was added to the lower chamber. After 24 hours, cells remaining on the upper membrane were removed with cotton wool. Cells that had migrated or invaded through the membrane were stained with the crystal violet (0.5%, Sigma) after fixation with 4% PFA as described above. Stained cells were then photographed and counted using ImageJ.

QUANTIFICATION AND STATISTICAL ANALYSIS

We used either a parametric or a nonparametric test of statistical significance on the basis of whether the data were normally distributed. Multiple comparisons were made by ANOVA. R, Excel (Microsoft) and Prism (GraphPad) were used for statistical analyses. Statistical significance was defined as a $P < 0.05$. P-values were shown on the figures as *asterisks*: *, $P < 0.05$; **, $P < 0.01$; ***, $P < 0.001$; ****, $P < 0.0001$. Independently performed biological replicates (n values) are indicated as circles in the bar graphs.